uOttawa

L'Université canadienne
Canada's university

FACULTÉ DES ÉTUDES SUPÉRIEURES ET POSTOCTORALES

uOttawa

L'Université canadienne
Canada's university

FACULTY OF GRADUATE AND POSDOCTORAL STUDIES

Susan Watson
AUTEUR DE LA THÈSE / AUTHOR OF THESIS

M.A.Sc. (Electrical Engineering)
GRADE / DEGREE

School of Information Technology and Engineering
FACULTÉ, ÉCOLE, DÉPARTEMENT / FACULTY, SCHOOL, DEPARTMENT

A Spherical Subspace Tracker with Adaptive Rank Estimation for Detection of Phase-modulated Signals

TITRE DE LA THÈSE / TITLE OF THESIS

M. Bouchard
DIRECTEUR (DIRECTRICE) DE LA THÈSE / THESIS SUPERVISOR

J-Y. Chouinard
CO-DIRECTEUR (CO-DIRECTRICE) DE LA THÈSE / THESIS CO-SUPERVISOR

EXAMINATEURS (EXAMINATRICES) DE LA THÈSE / THESIS EXAMINERS

C. D'Amours

R. Goubran

Gary W. Slater
LE DOYEN DE LA FACULTÉ DES ÉTUDES SUPÉRIEURES ET POSTDOCTORALES /
DEAN OF THE FACULTY OF GRADUATE AND POSTDOCORAL STUDIES

A SPHERICAL SUBSPACE TRACKER WITH ADAPTIVE RANK ESTIMATION FOR DETECTION OF PHASE-MODULATED SIGNALS

by

Susan Watson

Thesis submitted to the

Faculty of Graduate and Post-Doctoral Studies

in partial fulfillment of the

Master's of Applied Sciences

in Electrical Engineering

Master's Thesis

Ottawa-Carleton Institute of Electrical and Computer Engineering

School of Information Technology and Engineering

Faculty of Engineering

University of Ottawa

January 2005

Your file Votre référence
ISBN: 0-494-11452-5
Our file Notre référence
ISBN: 0-494-11452-5

Abstract

In this thesis, detection algorithms for cellular wireless communication are presented, which track the dominant eigenvalues and eigenvectors of the multipath fading channel. A decision variable may be formed from these eigenvectors and eigenvalues which uses the multipath diversity inherent in the channel, as well as advantageously combines orthogonal (uncorrelated) signal components. The determination of the rank of the signal-noise subspace is effected in the algorithms in two different ways; in the first, by calculation of an information criterion giving the probable dimension, and in the second, by choosing the dimension which includes a given percentage of the signal energy. Realistic simulations using measured channel impulse response data show a small performance gain of the eigenanalysis detection algorithm over simple differential detection.

Acknowledgments

I would like to extend my sincere thanks to the following people for their support. My co-supervisors Dr. Martin Bouchard and Dr. Jean-Yves Chouinard provided me with considerable insight over the course of this endeavour. On several occasions, Jean-Yves took time out of his trips to Ottawa to meet with me at the University. Martin has also been very generous with his time, and I thank them both.

Thanks also to Dr. François Patenaude, who kindly provided me with the channel impulse data used in this thesis. It is upon his extremely elucidating PhD thesis that this work is largely based, and so I also owe him thanks for teaching me through his written work.

Thanks to the DE Society for lunchtime conversation, to Dave Fenton for moral support, and to Lech Szymanski for pro bono computer services.

Finally, special thanks to my fiancé Mike Ewing and my family.

Contents

List of Figures

List of Tables

List of Acronyms

Acronym	Definition
AIC	Akaike Information Criterion, or An Information Criterion
AWGN	Additive White Gaussian Noise
CRC	Communications Research Centre
COST	Cooperation in the field of Scientific and Technical Research
DPSK	Differential Phase Shift Keying
DS-CDMA	Direct Sequence Code Division Multiple Access
W-CDMA	Wideband Code Division Multiple Access
DSP	Digital Signal Processing
GSM	Global System for Mobile Communications
IIS	Inter-symbol Interference
IPI	Inter-path Interference
MDL	Minimum Description Length

MLSE	Maximum-Likelihood Sequence Estimation
PSK	Phase Shift Keying
WCDMA	Wideband Code Division Multiple Access
WSS	Wide Sense Stationary
WSSUS	Wide Sense Stationary Uncorrelated Scattering

List of Symbols

Symbol	Description
$\otimes$	convolution operator
$\lvert\cdot\rvert$	modulus
$\lVert\cdot\rVert$	Euclidean norm
α	exponential weighting constant used in the update of $\mathbf{R}_{n-1}$
α_j	diagonal element of a tridiagonal matrix
$\mathbf{a}_n$	column vector of the D complex gains at time t_n
$a_d(t)$	complex gain of the d^{th} path at time t
$A_d(t)$	magnitude of $a_d(t)$
A	a general square, symmetric matrix
a_{ij}	element in the i^{th} row and j^{th} column of the matrix A
β_j	sub-diagonal and super-diagonal element of T_j
b_n	binary symbol at time t_n

B_f	bandwidth of the receiver input filter
B_d	Doppler spread
B_s	signal bandwidth
B	lower triangular matrix; part of the Cholesky factorization $\mathsf{B} \cdot \mathsf{C}$
c	speed of light; 3×10^8 m/s
C_N	constant used for information criterion
C	upper triangular matrix; part of the Cholesky factorization $\mathsf{B} \cdot \mathsf{C}$
d	index of paths
$\hat{d}$	estimated dimension of the signal+noise subspace
D	number of paths in the impulse response
$D(t)$	time-varying number of paths in the impulse response
D_{MDL}	number of paths given by the MDL criterion
D_c	number of paths given by the maxima in the power delay profile
D_{eff}	effective diversity according to the power delay profile
$D_{eff-ortho}$	effective orthogonal diversity according to the normalized eigenvalues l'_d
$D_{x\%}$	number of orthogonal modes necessary to represent $x\%$ of the total energy
$\mathbf{D}_{n-1}$	diagonal matrix of eigenvalues of $\mathbf{R}_{n-1}$ with spherical noise subspace
δ_k	k^{th} eigenvalue of $\mathbf{R}_s$

$\delta(t)$	impulse function at time t
$(\Delta f)_c$	coherence bandwidth
e	constant: 2.718281828 ...
$E[X]$	expectation of random variable X
E_b	energy per bit
$\mathbf{e}_n$	column vector made from the last $K-D$ elements of $\mathbf{q}_n$
η_i	square root of the i^{th} eigenvalue of $\mathbf{R}_n$
$\eta_h(t)$	time-varying mean of random process h(t)
$f(t)$	transmit filter; for DS-SS signals, a pseudonoise sequence
f_c	carrier frequency
f_d	Doppler shift
$\mathbf{G}_n$	diagonal matrix applied to $\mathbf{x}_n$
$\mathrm{g}_i^{(j)}$	eigenvectors of T_j at j^{th} iteration of Lanczos method
$\Gamma(m)$	the complete gamma function evaluated at m
$h(\tau;t)$	time-varying impulse response
$\mathbf{h}_n$	sampled impulse response at time t_n
$\hat{\mathbf{h}}_n$	estimated impulse response at time t_n
$\mathbf{H}_n$	transformation matrix for $\mathbf{q}_n$
$\mathbf{H}_{K-D}^{(v)}$	Householder matrix for $\mathbf{e}_n$
$\Im(\cdot)$	imaginary part of $\cdot$

$\mathbf{I}_K$	identity matrix of size $K \times K$
l_i	eigenvalues of the matrix $\hat{\mathbf{R}}$
l_i'	normalized eigenvalues of the matrix $\hat{\mathbf{R}}$
L	general lower triangular matrix used in the QL decompostion of A
$L(\hat{d})$	likelihood function, in $\hat{d}$
λ_k	k^{th} eigenvalue of $\mathbf{R}_n$
$\mathbf{\Lambda}$	diagonal matrix of the eigenvalues of $\mathbf{R}$
N	number of vectors involved in the formation of the autocorrelation matrix
N	dimension of the matrix A
$p(t)$	combined response of the transmit and receive filters $f(t) \otimes q(t)$
$p(\tau)$	impulse-like waveform; a very short pulse
P_e	bit error probability
$\mathbf{p}[\tau_d(t_n)]$	column vector, formed from samples in τ of $p(\tau - \tau_d(t_n))$
$\mathbf{P}(t_n; \tau_k)$	matrix at time t_n whose column vectors are $\mathbf{p}[\tau_d(t_n)]$
$\mathbf{P}$	fixed matrix whose columns are $\mathbf{p}[\tau_d(t_n)]$
$\mathsf{P}^{(\mathsf{k})}_{\mathsf{n-1,n}}$	plane rotation designed to eliminate $\mathsf{a}_{\mathsf{n-1,n}}$
$\mathcal{P}$	projection matrix for the noise subspace
π	constant: 3.141592654 ...
$q(t)$	matched (receive) filter

Q	unitary orthogonal matrix
$\mathsf{Q_j}$	matrix of Lanczos vectors at iteration j
$\mathsf{q_j}$	Lanczos vectors at iteration j
$\mathbf{q}_n$	real vector calculated from $\mathbf{q}_n$
$\mathbf{r}_n$	sampled received vector for the symbol arriving at time t_n
$\mathsf{r_j}$	residual at iteration j of Lanczos algorithm
$r(n)$	number of eigenvalues and eigenvectors being tracked at time t_n
$r'(t)$	received signal before filtering
$r''(t)$	received signal after filtering with q(t)
$r_s(n)$	estimated number of dominant eigenvalues and eigenvectors at time t_n
$\mathbf{R}$	ideal autocorrelation matrix of $\mathbf{r}_n$ or $\mathbf{h}_n$
R	general upper triangular matrix used in the QR decomposition of A
$\mathbf{R}_n$	estimated autocorrelation matrix of $\mathbf{R}$ at time t_n
$\hat{\mathbf{R}}$	estimated autocorrelation matrix of $\mathbf{R}$
$R_h(t_1, t_2; \tau_1, \tau_2)$	general autocorrelation function of $h(\tau; t)$
$R_h(\Delta t; \tau)$	autocorrelation function of $h(\tau; t)$ under the assumption of stationarity
$\Re(\cdot)$	real part of $\cdot$
$\rho(\tau)$	power delay profile

$s(t)$	received signal in complex baseband form
$s_{lp}(t)$	low pass equivalent of $s_{bp}(t)$
$s_{bp}(t)$	received bandpass signal
s_k	shift applied at the k^{th} iteration of the QR algorithm
$S(f;\tau)$	scattering function of the channel impulse response
$\mathbf{S}_n$	rank-one update of $\mathbf{\Lambda}_{n-1}$
$\mathbf{s}_n$	real vector calculated from $\mathbf{q}_n$
$theta_d(t)$	phase of $a_d(t)$
t	observation time variable
t_n	time of arrival of the n^{th} symbol; $t_n = nT_{time}$
T_m	delay spread
T_c	coherence time
T_f	length in time of filter $f(t)$
T_{delay}	sampling time in τ
T_{time}	sampling time in t
T_j	tridiagonal matrix at iteration j of Lanczos algorithm
τ	delay variable; relative to t
τ_k	delay at the k^{th} sampling time; $\tau_k = kT_{delay}$
$\tau_\mathsf{i}^{(\mathsf{j})}$	eigenvalues of T_j
$\tau_d(t)$	delay of the d^{th} path at time t_n

$\upsilon'(t)$	baseband additive noise of $r'(t)$
$\boldsymbol{\upsilon}_n$	column vector of white Gaussian noise samples
U_n	decision variable for symbol arriving at time t_n
$\mathbf{U}_n$	eigenvector matrix for $\mathbf{S}_n$ at time t_n
μ	eigenvalue for which we seek the corresponding eigenvector using inverse iteration
ν	doppler shift
V	mobile velocity
$\mathbf{v}_k$	k^{th} eigenvector of $\mathbf{R}$
$\mathbf{V}$	eigenvector matrix; columns are the eigenvectors $\mathbf{v}_k$
$\mathbf{V}_n$	eigenvector matrix at time t_n
$\mathbf{V}_{(s)}$	matrix whose columns are the signal+noise eigenvectors
$\mathbf{V}_{(\upsilon)}$	matrix whose columns are the noise eigenvectors
v_k	interim vector used to calculate x_k
$\mathbf{x}_n$	complex vector calculated by projecting $\mathbf{r}_n$ onto $\mathbf{V}_{n-1}^H$
x_k	pre-cursor vector to the eigenvector of T_j at iteration k of inverse iteration procedure
$\mathsf{y}_\mathsf{i}^\mathsf{j}$	Ritz vectors at iteration j of Lanczos algorithm
z^j	pre-cursor vector to the Lanczos vector at j^{th} iteration of Lanczos algorithm

Chapter 1

Introduction

Mobile telecommunications has been subject to large-scale growth precipitating the need for enhanced, more efficient systems. To meet the projected demand for broadband mobile services, research and development of third generation (3G) technologies is ongoing. The aim is to provide wideband services at data rates as high as 2 Mb/s with the same quality as wireline networks. Based on direct sequence code division multiple access (DS-CDMA), wideband CDMA (W-CDMA) is one such third generation system that is expected to become a global standard.

With high-bandwidth signalling as in W-CDMA, the mobile radio communications channel can be considered frequency selective; certain frequency components of the transmitted signal experience greater gains than others. Frequency selectivity is due

to the occurence of multipath fading; the effect whereby the transmitted signal travels to the receiver along a number of different paths, which have time-varying gains and delays. While a frequency selective channel does present more of a challenge to the system designer, there are means of mitigating the losses. In theory, the capacity of an infinite-bandwidth multipath fading channel is equal to that of an infinite bandwidth additive white Gaussian channel with the same signal to noise ratio without fading. By using diversity reception in the presence of fading, the performance of the system can be greatly improved.

To further define the challenges posed by frequency selective channels, a brief foray into the area of fading channels is in order. Certain existing methods of diversity combining for mitigation of frequency selective fading will be discussed, and their limitations.

1.1 Fading Channels

The time-variant nature of the channel is often described in terms of two types of variation: short-term fading and long-term fading. Short-term fading statistics of the received signal complex envelope (over a few tens of wavelengths) are usually assumed to be wide sense stationary. The long-term statistics (over a period of minutes) are the result of the mean variation of the received signal envelope, and are considered slow enough to be fixed over the short term [Ste87]. The short-term statistical nature of mul-

tipath fading channels is well explained in terms of a set of interfering waves [Cla68]. Assume that incident waves arrive with uniformly distributed random angles with respect to the receiver. Though the signals arrive very shortly after one another and though they may be close to equally attenuated, their phases can be quite different. This is due to the fact that the carrier phase is very sensitive to the path length; high-frequency signals can change in phase by 180 degrees over a very short distance. The phase distribution can be assumed to be uniform over $[0, 2\pi)$. The result is that the complex received waveform, the vector sum of all the paths arriving at one time, is a random variable. The sum can be a net gain or a net loss; when the modulus of the signal is very low this is called a fade. During a fade the channel noise may be higher than the signal, resulting in bit errors.

The received signal at a given time being the vector sum of all the contributions of the individual paths, then by the central limit theorem, the statistics of the real and imaginary parts of the complex envelope of the received waveform are Gaussian. That makes the magnitude of the complex envelope Rayleigh distributed, as it is the sum of the squares of two zero-mean, equal variance Gaussian random variables. If X is the random variable describing the magnitude of the complex path gains, then the probability density function of the complex envelope is given by the Rayleigh distribution:

$$P_X(x) = \begin{cases} \frac{x}{\sigma^2} e^{\frac{-x^2}{2\sigma^2}}, & \text{for } x \geq 0, \\ 0, & \text{for } x < 0. \end{cases} \tag{1.1}$$

If in addition to the scattered incident waves, there is a single powerful wave from the transmitter to the receiver without obstruction, this is called a line of sight path. With the existence of a line of sight path, the envelope distribution becomes Rician. This can be represented by two Gaussian processes in quadrature, as in the Rayleigh distribution case, but with at least one non-zero mean component. Thus the Rician distribution is a more general distribution which includes the Rayleigh distribution as a special case. The Rician probability density function is expressed as:

$$P_X(x) = \begin{cases} \frac{x}{\sigma^2} e^{\frac{-(x^2+A^2)}{2\sigma^2}} I_0\left(\frac{Ax}{\sigma^2}\right), & \text{for } A \geq 0, x \geq 0, \\ 0, & \text{for } x < 0. \end{cases} \tag{1.2}$$

The parameter A in the Rician distribution denotes the peak amplitude of the dominant path, and I_0 represents the modified Bessel function of the first kind of order zero. Often the line of sight path is characterized with a parameter K, which is defined as the ratio between the power in the LOS path and the variance of the multipath, ie, $K = \frac{A^2}{2\sigma^2}$.

Another useful statistical model for the complex envelope of the channel response is the Nakagami-m distribution, the pdf of which is as follows:

$$P_X(x) = \frac{2}{\Gamma(m)} \left(\frac{m}{\Omega}\right)^m x^{2m-1} e^{mx^2/\Omega} \tag{1.3a}$$

$$m = \frac{\Omega^2}{E[(X^2 - \Omega)^2]}, m \geq 1/2 \tag{1.3b}$$

$$\Omega = E[X^2] \tag{1.3c}$$

This distribution has two variables; m and Ω. Nakagami m-fading is a general fading distribution, the form of which is varied with the parameter m. With $m = 1$, the distribution reduces to the Rayleigh fading case. As m is increased, the fading becomes less severe. Based on measured channel impulse response data, the Nakagami-m distribution is a good fit. However, for practical purposes Rayleigh or Rician fading models are sufficiently realistic [BD91]. The simulated channels in this thesis will be limited to having either Rayleigh or Rician fading.

1.2 Correlated Diversity Branches

A simple way to mitigate fading due to time dispersion is to use a RAKE receiver. The conventional RAKE receiver attempts to gather up a number of delayed echoes of the transmitted signal and use them to compensate for signal loss. If the received copies had arrived via independently fading channels, the probability that all D copies were attenuated below a certain value is p^D, where p is the probability that any one

signal will fade below that value. Thus, the performance of the receiver benefits from the inherent channel multipath diversity.

While diversity gain can best be achieved with independent diversity branches, in practice, there is some amount of correlation between the channel paths. Channel diversity is compromised by certain propagation effects, namely:

- signals arriving after having been reflected from a common surface,
- signals arriving within a time period too small to be resolved by the receiver,
- diffracted and refracted signals arriving continuously within a time interval.

It stands to reason that these effects would take a toll on the performance of a diversity receiver such as the RAKE, depending on the degree of correlation. Correlation coefficients between amplitudes of paths within a multipath profile have been the subject of several studies. Turkmani [TDP91] and Hashemi [Has93a] found low correlation coefficients between paths when considering the small-scale fluctuations, for their outdoor urban and indoor channel impulse response measurements respectively. However, other studies (e.g. [JFT+72], [Baj68]) report correlations of up to 0.6 in conventional cellular environments, and [Pat96] reports correlation coefficients ranging from 0 to higher than 0.8 for a variety of environments.

Where the complex path gains are uncorrelated and there is no pulse overlap due to insufficient resolution at the receiver, the autocorrelation of the channel impulse response would be diagonal. This would indicate an orthogonal basis for the channel impulse reponse; the ideal scenario from a diversity viewpoint. There is evidence however to indicate that the degree of correlation between amplitudes of adjacent multipath components in the channel impulse response is significant. Still, by performing the eigenanalysis of the estimated channel autocorrelation matrix, an orthogonal basis of signal-space vectors and their corresponding powers is revealed. Then these eigenvalues and eigenvectors of the autocorrelation matrix of the received signal can be used for detection. This is the concept of an orthogonal diversity combining detector, the analysis of which is the subject of this thesis.

1.3 Thesis Objectives and Organization

This thesis presents performance results and complexity analysis of a RAKE-like detector structure whose branches consist not of the received delayed signal copies, but of the orthogonal eigenvectors of the autocorrelation of the received signal. Maximal ratio combining is used, but using eigenvalues as branch weights since these are the orthogonal complex gain powers of each path. The contributions of this thesis are as follows. Previously, the detection algorithm was conceived on the basis of results found regarding the orthogonal effective diversity of several types of mobile radio channels. In

this thesis, the basic algorithm is further developed to allow the eigenstructure to be updated with a greater or lesser number of modes than the previous iteration. This is a necessary refinement of the existing algorithm if the benefits of a reduced dimension channel are to be fully exploited. Results presented include a demonstration of the performance advantage of the detection algorithm, and information as to the speed of execution as it executes on a DSP processor in real-time. As the number of instructions and hence, speed of execution can vary with the particular eigendecomposition algorithm used, two different algorithms are implemented and compared.

The detector is tested using standard simulated Rayleigh channels such as COST-207, with varying fading rates. The COST-207 and COST-259 channels have a fixed number of Rayleigh-distributed paths with fixed delays. Being that the detection algorithm is an adaptive one, it is desirable to test it on a realistic random channel. Having had the fortune to be provided with many series of actual channel impulse response measurements[1], tests are run with actual channel data. Three types of environments are considered; an indoor (office building) channel, a typical cellular channel and a microcellular channel, where the base station transmitter is closer to ground-level and there is a line of sight path.

[1]Thanks again to Dr. Patenaude and the Communications Research Centre (CRC) for providing the channel impulse response data.

The organization of the thesis is as follows. Chapter 2 presents some previous work in the areas of channel modelling and diversity detection. Chapter 3 introduces the detection algorithm given in [Pat96], and the proposed additions to the algorithm. Also the chosen eigendecomposition algorithms are outlined (QR algorithm and Lanczos method), and a complexity analysis of the entire detection process is given. In chapter 4, the results of the simulations are presented for the simulated channels as well as for the channels based on impulse response measurements. Lastly, chapter 5 summarizes the thesis results, indicates the contributions of the thesis, and suggests further research studies.

Chapter 2

Channel Modeling by Eigenanalysis

2.1 Introduction

The success of a receiver design is intimately linked with the knowledge of the particular channel for which it is conceived. The design for the detector presented in chapter 3 is motivated by the results of study in the area of mobile radio channel modelling using eigenanalysis. Particularly significant is the observation that the impulse response of a frequency-selective fading channel can be represented by a small number of orthogonal modes of propagation. In this chapter, some results in the eigenanalysis of wideband fading channel impulse response measurements are presented. Prior to that,

some fundamental concepts involving the mobile radio channel model are discussed.

2.2 Impulse Response of a Mobile Radio Channel

A mathematical representation of the channel impulse response of a mobile radio channel is now considered. Assume that there are a finite number of propagation paths, $D(t)$, supported by the channel. Defining a time variable, τ, called the delay to measure the time of arrival of a given signal copy with respect to the time of the beginning of signal transmission, a model of the multipath channel impulse response in lowpass equivalent form is:

$$h(t;\tau) = \sum_{d=1}^{D(t)} a_d(t)\delta(\tau - \tau_d(t)) \tag{2.1}$$

where $a_d(t) = |a_d(t)|e^{j\theta_d(t)}$ is the complex gain of the d^{th} path. The impulse response is a function of both the observation time t and delay τ. The response of the channel to a signal transmitted at one time is not the same as the response to the same signal at a later time; it is time-variant. Random parameters include the number, delay and complex gains of the strong peaks in the impulse response.

The amount of scattering and diffraction involved in the propagation process makes for a continuous system function, as the multipath signals can arrive arbitrarily close to one another in time. This situation is reflected in the continuous time equation 2.1 above. However, for the purposes of a channel representation that will eventually be

useful in developing a detection algorithm, it must be recognized that communications systems have finite delay resolution. From the perspective of the receiver, two paths whose difference in time delay is less than $1/B_s$ where B_s is the transmission bandwidth cannot be resolved, and are observed as one path. Thus all paths arriving within the range $\tau_k \leq \tau \leq \tau_{k+1}, k \in I$ will be considered the same path, with $\tau_{k+1} = \tau_k + 1/B_s$ and $\tau_0 = 0$. The path complex gains are referred to in this context; they are the gains of each of the resolvable paths given that there is a smallest discernable time unit.

A fundamental characteristic of the channel, the delay spread, is the time difference between the delay of the first path and the delay of the D^{th} (and final) path. The relationship between the delay spread and the duration of the transmitted data pulse is important. If the data pulse duration is longer than the delay spread, the signal sprectrum will be negligibly affected by its transmission through the channel. However, if the data pulse duration is much smaller than the delay spread, the signal spectrum undergoes frequency selective fading. Another parameter which is often used when discussing delay spread is called the coherence bandwidth and is defined as:

$$(\Delta f)_c \triangleq \frac{1}{T_m} \tag{2.2}$$

with the delay spread denoted by T_m. The coherence bandwidth can be loosely interpreted as the bandwidth over which the channel can be considered equal gain and linear phase.

The fact that objects affecting the channel response are in motion – the receiver itself as well as scatterers – manifests itself in a phenomenon known as Doppler spread. The Doppler spread is a measure of the spectral broadening caused by the rate of change of the random variables $a_d(t)$. If a pure tone f_c is transmitted through the channel, it will undergo frequency dispersion and the received signal will have frequency components in the range $f_c - f_d$ to $f_c + f_d$, where f_d is the Doppler shift. The Doppler shift is a function of the velocity of the mobile and the angle of incidence of the incoming wave with respect to the direction of motion of the mobile. A measure of the time over which the frequency dispersion is assumed to be approximately constant is the coherence time:

$$T_c \approx \frac{1}{f_d} \tag{2.3}$$

Referring to Figure 2.1, which shows an example of a multipath fading channel, the delay spread can be seen to be approximately $2.5\mu s$. The variance in the path gains $a_d(t)$ may clearly be seen, as well as the fact that the path delays $\tau_d(t)$ tend to be fairly constant.

2.2.1 Wide-Sense Stationary Uncorrelated Scattering Model

In addition to being time-varying, the mobile radio channel is a stochastic process. Notably, there are a few assumptions that can be made regarding the stationarity of the radio channel statistics, as well as some observations on the correlation function of the channel impulse response. Channels that exhibit both time and frequency fading can

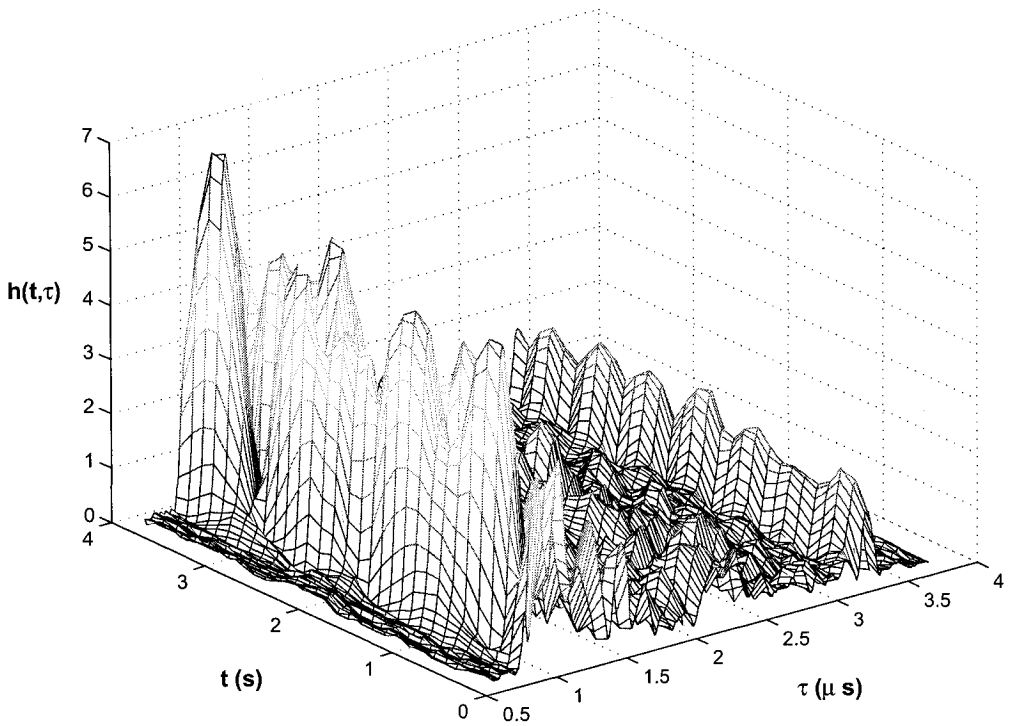

Figure 2.1: Multipath fading: time-varying impulse response

be approximated by the wide-sense stationary uncorrelated scattering (WSSUS) model. Consider the channel impulse response as a set of random processes in time, indexed against the path delay variable. Or equivalently, a set of random filter processes, indexed against the Doppler shift (a frequency variable related to the time delay).

For a random process in time to satisfy the wide-sense stationarity requirement, its mean and autocovariance must be independent of absolute time. So for each time delay in the channel impulse response, it is assumed that the random process has a constant mean:

$$\eta_h(t)|_{WSS} = \eta_h \tag{2.4}$$

and the autocorrelation must be invariant under a time shift, and therefore depend only on the difference in time:

$$R_h(t_1, t_2; \tau_1, \tau_2) = E[h(t_1, \tau_1)h^*(t_2, \tau_2)] \tag{2.5}$$

$$R_h(t_1, t_2; \tau_1, \tau_2)|_{WSS} = R_h(\Delta t; \tau_1, \tau_2), \Delta t = t_2 - t_1 \tag{2.6}$$

Now if the complex path gain process at delay τ_1 is uncorrelated with the complex path gain process at delay τ_2, then this situation is called uncorrelated scattering. With the addition of uncorrelated scattering to the WSS stipulation, one arrives at:

$$R_h(t_1, t_2; \tau_1, \tau_2)|_{WSSUS} = R_h(\Delta t; \tau_1)\delta(\tau_1 - \tau_2) = R_h(\Delta t; \tau) \tag{2.7}$$

Though the WSSUS channel is a useful theoretical model for the statistics of the channel impulse response, it is unfortunately not all that accurate. First of all, the complex gain processes are subject to the fluctuations in the environment as time passes such that their statistics cannot always be stationary. A channel in which the short-term statistics only are WSSUS is called a quasi-WSSUS channel [Bel63]. Secondly, as it was seen previously, in reality there exists correlation between the complex path gains.

2.2.2 Functions of the Channel Impulse Response

Referring to (2.6), the autocorrelation function under the assumption of wide-sense stationarity in time, evaluated at $\Delta t = 0$ gives the autocorrelation function of the complex gains. Now when a further stipulation of $\tau_1 = \tau_2$ is made, the result is the delay power profile.

$$\rho(\tau) = E[|h(t;\tau)|^2]\Big|_t \tag{2.8}$$

Figure 2.2 is an example of a power delay profile; it represents the average power in each path versus the delay. It is also called the multipath intensity profile in the literature. The power delay profile is pertinent to our discussion as it provides a first estimate of the number of dominant paths in the channel. One can define D_c as the number of maxima in the delay power profile that exceed some minimum power threshold, for example, -20 dB.

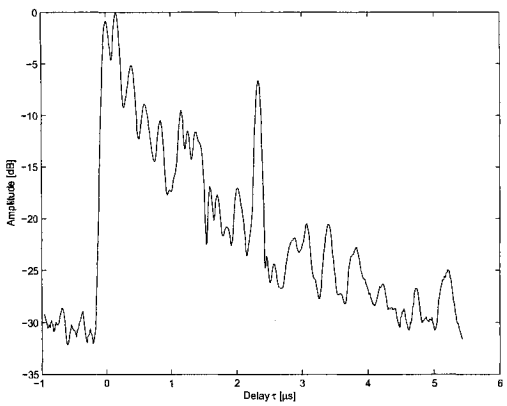

Figure 2.2: Power-delay profile for a cellular channel. Source: CRC data, cc721.mat.

A set of useful functions for characterization of the Doppler spread and delay spread of the channel arises when the Fourier transform of the autocorrelation function is examined in dual domains. The delay variable, τ, in the impulse response corresponds to a frequency f. The dual of time t is a frequency ν in the Doppler shift domain. Starting with the autocorrelation of a WSSUS channel, if one takes the Fourier transform with respect to delay,

$$\begin{aligned} R_H(f_1, f_2; \Delta t) &= \int_{-\infty}^{\infty} \int_{-\infty}^{\infty} R_h(\Delta t; \tau_1) \delta(\tau_1 - \tau_2) e^{j2\pi(f_1\tau_1 - f_2\tau_2)} d\tau_1 d\tau_2 \\ &= \int_{-\infty}^{\infty} R_h(\Delta t; \tau_1) e^{j2\pi(f_1 - f_2)\tau_1} d\tau_1 \\ &= \int_{-\infty}^{\infty} R_h(\Delta t; \tau_1) e^{j2\pi(\Delta f)\tau_1} d\tau_1 \\ &= R_H(\Delta f; \Delta t) \qquad \text{where } \Delta f = f_2 - f_1 \end{aligned} \tag{2.9}$$

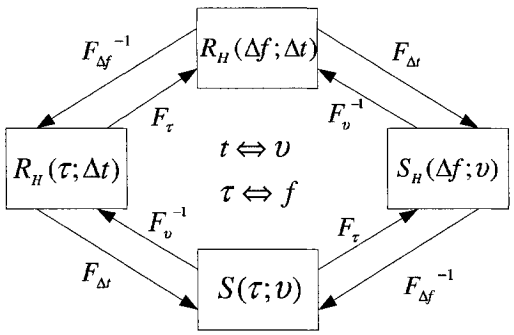

Figure 2.3: Interrelationships between correlation functions.

the result is a three-dimensional correlation function with variables representing the time difference and the frequency difference. It is called the spaced-frequency, spaced-time correlation function of the channel [Pro01].

If one takes the Fourier transform of this function with respect to Δt, the result is the function $S_H(\Delta f;\nu)$.

$$S_H(\Delta f;\nu) = \int_{-\infty}^{\infty} R_H(\Delta f;\Delta t)e^{j2\pi\nu\Delta t}d\Delta t \tag{2.10}$$

$S_H(\Delta f;\nu)$ is a function relating the time variations of the channel to Doppler effects. If one performs the same operation on the autocorrelation function $R_h(\Delta t;\tau_1)$, one obtains:

$$S(\tau;\nu) = \int_{-\infty}^{\infty} R_h(\Delta t;\tau)e^{j2\pi\nu\Delta t}d\Delta t \tag{2.11}$$

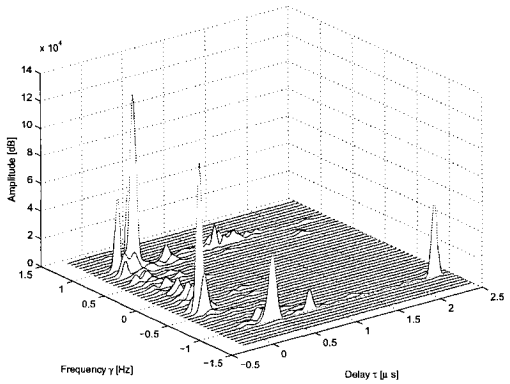

Figure 2.4: Scattering function for a cellular channel. Source: CRC data, cc721.mat.

This function, $S(\tau;\nu)$, is called the scattering function of the channel. It shows the fading spectrum at a given delay; see Figure 2.4. At a constant delay, the fading spectrum will generally have over the short term only a small number of dominant peaks. It is possible to identify the angles of arrival of these dominant components, since the relationship between the frequency and the angle of arrival α is:

$$f_D = \frac{V}{c} f_c \cos\alpha \tag{2.12}$$

where V is the mobile velocity, c is the speed of light and f_c is the carrier frequency.

2.3 Mobile Radio Channel Modelling

There have been many influential works in the area of mobile channel modelling. Bello [Bel63] regarded the channel as a set of randomly time-varying linear filters, and

gave a theoretical description in terms of interrelated system transfer functions in time and frequency. Bello's work complemented more empirical studies, such as that of Cox [Cox72] and others. Cox first conducted a series of impulse response measurements in New York City, using a channel sounder based on spread-spectrum modulation (described in Appendix A). In Cox's work and Bajwa's [Baj68] the average delay-power profiles of various locations were presented, as the average delay spread and Doppler spectra. The two-dimensional scattering function mentioned above was useful in identifying individual propagation paths, from their angles of arrival. Turin's approach [JFT+72] to analysis of channel sounding data was to attempt to find the probability distributions of the channel parameters such as the path gains $A_i(t)$ and time delays $\tau_i(t)$.

The algorithms in this thesis will rely upon the characterization of the channel impulse response in terms of its dominant modes of propagation. As in previous studies, the channel impulse data comes from channel sounding experiments and is processed and analyzed to test for certain statistical criteria. A description of the analysis follows.

2.3.1 Channel Modelling by Eigenanalysis

An $N \times N$ covariance matrix $\mathbf{R}$ has the eigenvectors $\mathbf{V}$ and the eigenvalues $\mathbf{\Lambda}$ if

$$\mathbf{RV} = \mathbf{\Lambda V} \tag{2.13}$$

where

$$\mathbf{V} = \begin{bmatrix} \uparrow & \uparrow & & \uparrow \\ \mathbf{v}_1 & \mathbf{v}_2 & \cdots & \mathbf{v}_N \\ \downarrow & \downarrow & & \downarrow \end{bmatrix} \tag{2.14}$$

and

$$\mathbf{\Lambda} = diag\begin{pmatrix} \lambda_1 & \lambda_2 & \cdots & \lambda_N \end{pmatrix} \tag{2.15}$$

The number of non-zero eigenvalues of $\mathbf{R}$ will be equal to its rank. The eigenvectors and eigenvalues satisfy the Schur decomposition, which will be useful in this section to expand $\mathbf{R}$ into its eigenvector components.

$$\mathbf{R} = \mathbf{V}\mathbf{\Lambda}\mathbf{V}^H \tag{2.16}$$

The eigendecomposition of an autocovariance matrix, for example of several signal impinging on an antenna array over time, reveals the common underlying vibrational components in the array. In the literature there are several examples of the applications of eigendecomposition of a covariance matrix. They include direction of arrival analysis with input from a sensor array, retrieving overlapping echoes from radar backscatter [BSK85], and blind channel estimation and equalization. In our case, the goal of the eigendecomposition is to identify the number and form of the dominant modes of propagation in a frequency-selective multipath channel.

Impulse response measurements collected using the method of channel sounding via a sliding correlator yield a series of vectors $\{\mathbf{h}_n\}_{n=1,2,\cdots,N}$. Each of the vectors $\mathbf{h}_n$ represents the sampled impulse response measured at the observation time $t_n = nT$. Given a sampling period T_{delay}, the expression for each $\mathbf{h}_n$ can be derived from the estimated continuous time impulse response function. Assuming that the complex gains are constant over the time of a very short pulse $p(\tau)$, the estimated continuous time function at times $t_n = nT$ is:

$$h(t_n;\tau) = \sum_{d=1}^{D} a_d(t_n)p(\tau - \tau_d(t_n)) + \upsilon_n(\tau) \tag{2.17}$$

where τ is the excitation time delay, $a_d(t_n) = |a_d(t_n)|e^{j\theta_d}$ are the complex gains, $\tau_d(t_n)$ is the delay of the d^{th} resolvable path. $\upsilon_n(\tau)$ is a zero-mean white noise process with samples of variance σ_υ^2. Now if the signal is sampled at a rate $\tau_k = kT_{delay}$ the equation can be written in vector form:

$$\begin{aligned}\mathbf{h}_n = \begin{bmatrix} h(t_n,\tau_1) \\ h(t_n,\tau_2) \\ \vdots \\ h(t_n,\tau_K) \end{bmatrix} &= \begin{bmatrix} \mathbf{p}[\tau_1(t_n)] & \mathbf{p}[\tau_2(t_n)] & \cdots & \mathbf{p}[\tau_D(t_n)] \end{bmatrix} \begin{bmatrix} a_1(t_n) \\ a_2(t_n) \\ \vdots \\ a_D(t_n) \end{bmatrix} + \begin{bmatrix} \upsilon_n(\tau_1) \\ \upsilon_n(\tau_2) \\ \vdots \\ \upsilon_n(\tau_K) \end{bmatrix} \\ &= \mathbf{P}(t_n;\tau_k)\mathbf{a}(t_n) + \boldsymbol{\upsilon}(\tau_k)\end{aligned} \tag{2.18}$$

where the column vectors $\mathbf{p}$ are:

$$\mathbf{p}[\tau_d(t_n)] = \Big[p(\tau_1 - \tau_d(t_n)) \quad p(\tau_2 - \tau_d(t_n)) \quad \cdots \quad p(\tau_K - \tau_d(t_n))\Big]^T \tag{2.19}$$

Using the QWSSUS (Quasi-WSSUS) model, the path delays are fixed over an appreciable duration, and the vectors of $\mathbf{P}(t_n; \tau_k)$ no longer depend on t_n. The final equation is expressed in matrix form as:

$$\mathbf{h}_n = \mathbf{P}\mathbf{a}_n + \upsilon_n \tag{2.20}$$

The matrix $\mathbf{P}$ can be thought of as a set of channels (the paths in the multipath channel model) which may or may not be independent, and which are weighted by the path gain vector. At each discrete value of the time delay τ, each of the channels contributes to the resultant value of $\mathbf{h}_n$ at that particular delay. Ideally, all of the signal energy present across the channels could be separated from the noise and reclaimed at the receiver; eigendecomposition will help with this task. The autocorrelation matrix is:

$$\mathbf{R} = E[\mathbf{h}_n\mathbf{h}_n^H] = \mathbf{P}\mathbf{R}_a\mathbf{P}^T + \mathbf{R}_\upsilon \tag{2.21}$$

where $\mathbf{R}_a = E[\mathbf{a}_n\mathbf{a}_n^H]$ is the autocorrelation matrix of the complex path gains and $\mathbf{R}_\upsilon = E[\upsilon_n\upsilon_n^H] = \sigma_\upsilon^2\mathbf{I}_K$ is the autocorrelation of the additive white gaussian noise, and $\mathbf{I}_K$ is the $K \times K$ identity matrix. If $\mathbf{v}_k$ is the k^{th} eigenvector of $\mathbf{R}$ with associated eigenvalues $\lambda_1 \geq \lambda_2 \geq \cdots \geq \lambda_k \geq \cdots \geq \lambda_K$, then the autocorrelation matrix can also be expressed as:

$$\mathbf{R} = \sum_{k=1}^{K} \lambda_k \mathbf{v}_k \mathbf{v}_k^H \tag{2.22}$$

The eigenvectors $\mathbf{v}_k$ are the eigenvectors of the sum $\mathbf{P}\mathbf{R}_a\mathbf{P}^T + \mathbf{R}_v$. The column space of $\mathbf{P}\mathbf{R}_a\mathbf{P}^T$ is referred to as the signal subspace of $\mathbf{R}$. The matrix $\mathbf{R}_v$ is the noise subspace, and is orthogonal to the signal subspace. The signal subspace is of rank D; in other words, the matrix $\mathbf{P}\mathbf{R}_a\mathbf{P}^T$ has D linearly independent columns. The noise subspace is of rank K, so added together, their combined rank is always K. Therefore the effect of the noise is to increase the apparent dimension of the system. If an estimate D of the dimension of the signal subspace is known, the eigendecomposition of $\mathbf{P}\mathbf{R}_a\mathbf{P}^T$ can be approximated by the first D eigenvalues and eigenvectors of $\mathbf{R}$.

Suppose the eigenvalues of the matrix $\mathbf{P}\mathbf{R}_a\mathbf{P}^T$ are ordered such that $\delta_1 \geq \delta_2 \geq \cdots \geq \delta_k \geq \cdots \geq \delta_K$. Then $\delta_{D+1} = \delta_{D+2} = \cdots = \delta_K = 0$, since the rank of $\mathbf{P}\mathbf{R}_a\mathbf{P}^T$ is D. It follows that the eigenvalues λ_k are:

$$\lambda_k = \begin{cases} \delta_k + \sigma_v^2 & k = 1, \cdots, D \\ \sigma_v^2 & k = D+1, \cdots, K \end{cases} \tag{2.23}$$

Clearly, if the values of λ_k were as above, the dimension of the signal subspace could easily be found. It would suffice to find the index k after which the eigenvalues become a smaller, identical number. However, this analysis was done assuming perfect knowledge of the autocorrelation function. In reality only an estimate of the autocorrelation, $\hat{\mathbf{R}}$ is available, and in that case, the eigenvalues will all be different with high probability. Still, there are ways to estimate the signal subspace dimension from the eigenvalues of

$\hat{\mathbf{R}}$.

An estimate of the autocorrelation matrix of the channel impulse response based on a finite number N of observations is given by:

$$\hat{\mathbf{R}} = \frac{1}{N}\sum_{n=1}^{N} \mathbf{h}_n \mathbf{h}_n^H \tag{2.24}$$

For $\hat{\mathbf{R}}$ to be a reasonable estimate of $\mathbf{R}$, the random process $\mathbf{h}_n$ should be ergodic, meaning that its time average asymptotically approaches the ensemble average.

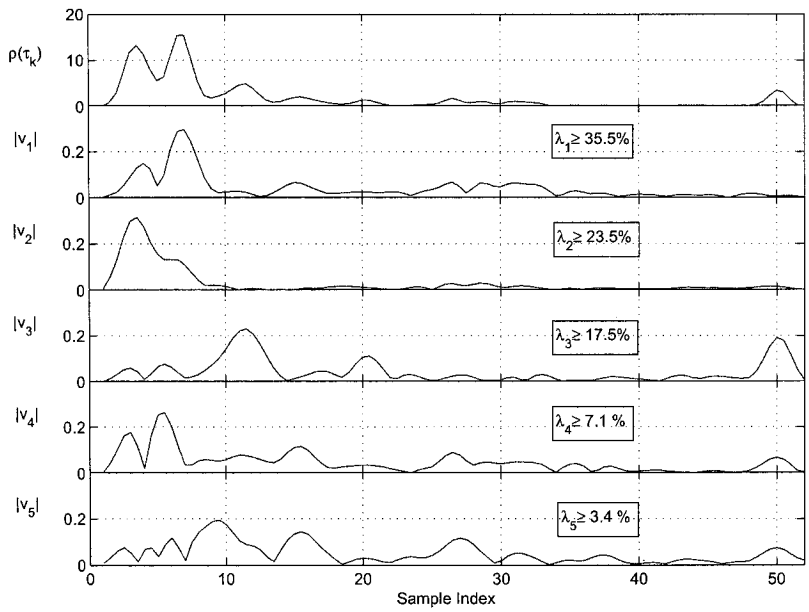

Figure 2.5: Power delay profile, eigenvector magnitudes and associated eigenvalues.

In Figure 2.5, the first five eigenvectors and eigenvalues are shown for the channel impulse response dataset cc721.mat. These eigenvalues and eigenvectors were found by first forming the autocorrelation matrix of the impulse response data, and then forming the eigenanalysis. The topmost graph depicts the power delay profile of the channel, which has a different scale than the rest of the graphs, which are the magnitudes of the eigenvectors. The power delay profile is shown for comparison, as the dominant peaks in this profile are identifiable in the eigenvectors. Note that the first 3 eigenvectors contain at least 76.5% of the signal energy, and that the 4th and 5th eigenvectors begin to resemble noise.

One strategy for estimating the signal subspace dimension from the estimated eigenvalues $\lambda_1 \geq \lambda_2 \geq \cdots \geq \lambda_k \geq \cdots \geq \lambda_K$ is to search the progression of the eigenvalues, looking for a break in the pattern whereby all larger eigenvalues can be attributed to the signal and all the smaller ones only to noise. This can be done with an information theoretic criterion [WK85] such as the Minimum Descriptive Length (MDL) criterion and the Akaike Information Criterion (AIC); the details of which will be given in Chapter 3. Note that the MDL and AIC criteria tend to overestimate the signal subspace dimension [Pat96].

Effective Orthogonal Diversity

The traditional way of counting the number of modes of propagation is to count the number of significant paths, D_c. However, if there is any pulse overlap, meaning if all the paths could not be resolved by the receiver, this measure would tend to underestimate the true diversity of the channel. The following diversity measures, originally proposed in [Pat96], aim to provide a more meaningful representation of a channel's diversity. The first of these is a measure of the number of signal subspace dimensions necessary to represent $x\%$ of the received signal energy. The λ_i are the eigenvalues of the matrix $\hat{\mathbf{R}}$.

$$D_{x\%} = \min_k \arg\left\{\left(\frac{\sum_{i=1}^{k}\lambda_i}{\sum_{i=1}^{K}\lambda_i}\right) > x/100\right\} \tag{2.25}$$

Now a problem still remains with D_c and $D_{x\%}$ as diversity measures; not all of the amplitudes of these paths are the same, which would give a falsely optimistic measure. Another measure is proposed, called the effective diversity is:

$$D_{eff} = D_c^{\sum_{d=1}^{D_c}\rho'(\tau')log_{D_c}\rho'(\tau'_d)} \tag{2.26}$$

where

$$\rho'(\tau'_d) = \frac{\rho(\tau'_d)}{\sum_{i=1}^{D_c}\rho(\tau'_i)} \tag{2.27}$$

Here the powers of each of the paths have been normalized with respect to the total power in all of the observed paths D_c. The exponent in (2.26) is reminiscent of the definition of entropy, if the normalized path amplitudes were thought of as probabilities.

Again here, this measure is susceptible to inaccuracy due to pulse overlap, and also to path gain correlation. A final diversity measure, which uses the eigenvalues of the matrix $\hat{\mathbf{R}}$ but in normalized form, will provide the most accurate measure: the effective orthogonal diversity, defined as:

$$D_{eff-ortho} = D_{x\%}^{-\sum_{d=1}^{D_{x\%}} \lambda'_d log_{D_{x\%}} \lambda'_d} \tag{2.28}$$

where the normalized eigenvalues are given by:

$$\lambda'_d = \frac{\lambda_d}{\sum_{i=1}^{D_{x\%}} \lambda_i} \tag{2.29}$$

The values of $D_{eff-ortho}$ can be greater than D_{eff} if there is pulse overlap, and less if the path gains are correlated. Some real-world results using the above diversity measures are tabulated in Table 2.1. For a description of the conditions under which the particular data presented was collected, see Appendix B. Note that in most cases $D_{eff-ortho}$ is lower than D_{eff}, indicating a certain degree of correlation. The signal subspace dimension D_{MDL} overestimates the actual diversity of the channel by a significant amount. The number of effective orthogonal modes of propagation supported by each type of channel is quite low, not exceeding 2 for indoor channels and 4 for urban channels.

From a detection standpoint, there are very interesting implications to these results. Since the number of maxima in the power delay profile is always higher than the effective diversity, there may be an advantage to a receiver that uses an orthogonal mode combining strategy instead of using the power profile to achieve a diversity gain.

Table 2.1: Measured diversity in the mobile radio channel

Parameter	Indoor 950 MHz	Indoor 40 GHz	Microcellular 910 MHz	Urban 910 MHz
D_c	3.3	2.5	1.5	7.4
D_{eff}	1.5	1.5	1.1	3.5
D_{MDL}	11	11	10	28
$D_{90\%}$	-	-	-	4.8
$D_{98\%}$	1.9	1.8	2.8	-
$D_{eff-ortho}$	1.2	1.2	1.4	3.2

2.4 Conclusion

The analysis of empirical data collected by channel-sounding experiments, as well as theoretical analysis, has given researchers a picture of the mobile radio channel under multipath fading. When examining the channel model using eigenanalysis, the primary modes of propagation can be characterized in terms of their eigenvectors and eigenvalues. The number of these primary modes is small, as indicated by the effective orthogonal diversity measure of actual channel data. There is the potential for an improved performance detector, enabled to find the orthogonal modes of the received signal to form a soft decision variable relatively uncorrupted by correlation.

Chapter 3

Eigenanalysis Detection Algorithm

3.1 Introduction

Observations of the mean impulse response of mobile radio channels in different environments has led to the discovery that most of the signal energy is borne by only a few modes of propagation. It has been postulated that it is be possible to create a detector which creates a decision variable based on a few orthogonal modes of the channel.

In this chapter, the operation of the eigenanalysis detector will be described, as well as the overall algorithm for constructing the autocorrelation matrix and tracking the

channel modes. Given the computational burden of the eigenanalysis, the complexity of the proposed detection scheme is one of the primary concerns, despite the reduced signal dimension in comparison to traditional RAKE detectors. Two different methods of performing the eigendecomposition will be proposed, and evaluated as to their complexity. By implementing and running the eigenanalysis detector in real-time, it is possible to further characterize the trade-off to be made between performance and complexity. In the next chapter the algorithms will be tested as to their performance in terms of bit error rate and profiled after compiler optimization.

3.2 Received Signal Vector

The following derivation relies upon the baseband equivalent form of a radio frequency signal. Otherwise known as the low-pass equivalent, this form can be related to the bandpass signal as follows:

$$s_{lp}(t) = s_{bp}(t)e^{-j2\pi f_c t} \tag{3.1}$$

where $s_lp(t)$ is the lowpass equivalent signal, which will be referred to hereafter as simply $s(t)$. After the frequency translation, the signal is then low-pass filtered. In actual implementation, the antenna output may be mixed down to baseband or an intermediate frequency and filtered using a superheterodyne receiver.

A commonly-used modulation technique for use with wireless channels is phase-shift keying (PSK). The transmitted signal waveform in baseband equivalent form is expressed as:

$$s(t) = \sum_{n=-\infty}^{\infty} b_n f(t - nT), \qquad b_n = \Re[e^{j2\pi(m-1)/M}] \qquad m = 1, 2, \cdots, M \tag{3.2}$$

where M is the number of possible modulation signals, and $f(t)$ is the pulse shape. Binary phase shift keying ($M = 2$) will be used in the performance simulations. The form of $f(t)$ must satisfy

$$E_b = \int_0^T f^2(t)dt = 1 \tag{3.3}$$

so that the energy per bit is normalized to 1.

It should be noted that $f(t)$, in the context of spread-spectrum systems, is the spreading code. Derived from it is its corresponding matched filter, $q(t)$. That is, the filter coefficients of $q(t)$ correspond to the time-reversed spreading code values. In a traditional RAKE receiver, a bank of these matched filters $q(t)$ are used, where each one is dedicated to filtering a signal with a given delay. In the case of the subspace-based receiver, a single code-matched filter is used, with the intent of separating the multipath components using eigenanalysis. It will now be seen how these multipath components manifest themselves in the received signal.

In the previous chapter, the impulse response of a mobile radio channel was discussed, and the model used was (2.1):

$$h(t;\tau) = \sum_{d=1}^{D(t)} a_d(t)\delta(\tau - \tau_d(t)) \tag{3.4}$$

with $a_d(t) = |a_d(t)|e^{j\theta_d(t)}$ the Rayleigh-distributed complex gains, τ is the excitation delay and $\tau_d(t)$ the specific delay of the d^{th} path. $D(t)$ is the number of paths. Consider the realized signal if the BPSK signal is sent over this channel, and include additive white Gaussian noise. The resulting signal is

$$\begin{aligned} r'(t) &= s(t) \otimes h(t;\tau) + v'(t) \\ &= \sum_{n=-\infty}^{\infty} b_n \int_{-\infty}^{\infty} f(t-\tau-nT) \sum_{d=1}^{D(t)} a_d(t)\delta(\tau - \tau_d(t))d\tau + v'(t) \\ &= \sum_{n=-\infty}^{\infty} b_n \sum_{d=1}^{D(t)} a_d(t) f(t - \tau_d(t) - nT) + v'(t) \end{aligned} \tag{3.5}$$

The form of this expression highlights the possibility that there may be copies of one transmitted symbol overlapping the signal for the next symbol; this is known as intersymbol interference (ISI). Let T_f be its duration in time of $f(t)$, the transmit filter (pulse shape). The condition to avoid intersymbol interference is:

$$\tau_d(t) + T_f \leq T, \qquad \forall\, d \tag{3.6}$$

meaning, the last copy of the transmitted symbol arrives before the next symbol begins. Another possible form of interference is interpath interference (IPI), and this occurs

when the time difference between the paths is smaller than the duration of a transmit symbol. The condition to avoid inter-path interference is:

$$|\tau_d(t) - \tau_i(t)| > T_f, \qquad \forall\, d \neq i \tag{3.7}$$

Usually, some amount of both IPI and ISI co-exist.

If the simplifying assumption is made that there is no ISI, the multipath arrivals fall within the time span of the symbol to be detected. The received signal during that time span can be expressed:

$$r'(t) = b_n \sum_{d=1}^{D(t)} a_d(t) f(t - \tau_d(t) - nT) + v'(t), \qquad nT \leq t < (n+1)T \tag{3.8}$$

This equation describes in general terms the unprocessed signal that will be used to reconstruct the symbol sent. The optimum detector for this type of signal is discussed in the next section. First, the detector must bandpass filter the signal to reject out of band noise, regardless of the structure of the receiver. Let the receiver input filter be $q(t) = f(-t)$; it represents a filter matched to $f(t)$.

$$\begin{aligned} r''(t) &= r'(t) \otimes q(t) \\ &= b_n q(t) \otimes \sum_{d=1}^{D(t)} a_d(t) f(t - \tau_d(t) - nT) + q(t) \otimes v'(t) \\ &= b_n \sum_{d=1}^{D(t)} a_d(t) p(t - \tau_d(t) - nT) + v(t), \qquad nT \leq t < (n+1)T \end{aligned} \tag{3.9}$$

where $p(t) = q(t) \otimes f(t)$ and $v(t) = q(t) \otimes v'(t)$. The noise signal $v(t)$ will no longer be white, since $q(t)$ is not likely to be a Nyquist filter.

Now in the case of a fairly slowly-fading channel, it is reasonable to expect that the path gains $a_d(t)$ and delays $\tau_d(t)$ will not change appreciably over the symbol duration. Then the path gains and delay functions can be expressed relative to time $t_n = nT$: $a_d(t_n)$ and $\tau_d(t_n)$. Their number, $D(t)$ can be considered fixed at D. Let us also introduce a delay variable representing the time since the start of the n^{th} symbol $\tau = t - nT$, $0 \leq \tau < T$. There is the underlying assumption that the receiver has synchronization circuitry to allow it to determine the beginning of a symbol. Then the received signal for the n^{th} symbol, over $nT \leq t < (n+1)T$ becomes:

$$r_n(\tau) = b_n \sum_{d=1}^{D} a_d(t_n) p(\tau - \tau_d(t_n)) + \upsilon_n(\tau) \tag{3.10}$$

This signal is sampled in delay every $\tau_k = kT_{delay}$, $T_{delay} = 1/2B_s$ is the sampling rate, and $k = 1, 2, ..., K$. The length-K vector $\mathbf{r}_n$ results. The variance of the noise samples is $E[|\upsilon_n(\tau_k)|^2] = \sigma_\upsilon^2 = N_0/T_{delay}$.

$$\mathbf{r}_n = b_n \mathbf{P}(t_n; \tau_k)\mathbf{a}_n + \boldsymbol{\upsilon}_n \tag{3.11}$$

where

$$\mathbf{a}_n = \begin{bmatrix} a_1(t_n) & a_2(t_n) & \cdots & a_D(t_n) \end{bmatrix}^T \tag{3.12}$$

$$\mathbf{P}(t_n; \tau_k) = \begin{bmatrix} \mathbf{p}[\tau_1(t_n)] & \mathbf{p}[\tau_2(t_n)] & \cdots & \mathbf{p}[\tau_D(t_n)] \end{bmatrix} \tag{3.13}$$

$$\mathbf{p}[\tau_d(t_n)] = \begin{bmatrix} p(\tau_1 - \tau_d(t_n)) & p(\tau_2 - \tau_d(t_n)) & \cdots & p(\tau_K - \tau_d(t_n)) \end{bmatrix}^T \tag{3.14}$$

$$\boldsymbol{\upsilon}_n = \begin{bmatrix} \upsilon_n(\tau_1) & \upsilon_n(\tau_2) & \cdots & \upsilon_n(\tau_K) \end{bmatrix}^T \tag{3.15}$$

The parameter K must be chosen depending on the particular channel conditions so as to retain the majority of the multipath information; to this end, K should be set to $\lceil \tau_{max}/T_{delay} \rceil$, where $\lceil \cdot \rceil$ is the ceiling function.

Empirical experiments show that path delays are more slowly varying that the actual path gains; in other words, when observing a power delay profile over time, each peak moves up and down in power more quickly than it drifts in delay. Put in more quantitative terms, if the fading is slow enough, in particular if $f_d(T + \tau_{max}) << 1$, the channel can be considered QWSS (Quasi-Wide Sense Stationary), and the structure of the channel can be considered constant over several symbol periods T. In this case, $\mathbf{P}(t_n; \tau_k)$ becomes simply $\mathbf{P}$, and the matrix form of the expression for the received

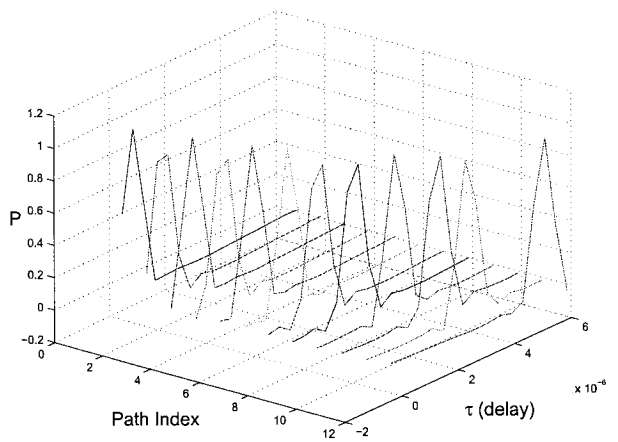

Figure 3.1: Example of the $\mathbf{P}$ matrix for a channel with 12 paths.

vector becomes:

$$\mathbf{r}_n = b_n \mathbf{P}\mathbf{a}_n + \boldsymbol{\upsilon}_n \tag{3.16}$$

There are several ways in which the above vector can be processed in order to extract the symbol, b_n. The classical approach is to use a RAKE detector. However, the RAKE detector is just one in a class of receivers utilizing the multipath channels' inherent diversity.

Spread-spectrum modulation lends itself to diversity reception, since the transmitted signal has a bandwidth much greater than the coherence bandwidth of the channel impulse response, which gives rise to its channel-sounding properties. Narrowband modulation techniques still benefit from the natural multipath diversity, but suffer more from interpath interference due to temporal dispersion [KM99]. Furthermore, CDMA systems make use of spread-spectrum modulation and are becoming a preferred solution for 3G cellular systems due to their high capacity. For these reasons spread-spectrum signals will be assumed throughout this work.

3.3 Eigenanalysis-based detector

In order to produce an autocorrelation matrix and extract the modes of the channel, it is necessary to preserve the parallelism that is introduced in the multipath channel. The incoming signal is filtered with the time-reversed spreading code as in the RAKE

detector, but instead of summing the output samples, the values of these individual samples are stored in the vector $\mathbf{r}_n$. These samples contain information about the location (in delay) and power of the most significant multipath components. One way to form the autocorrelation matrix is to use a uniform window as follows:

$$\mathbf{R}_n = \sum_{i=1}^{N} \mathbf{r}_i \mathbf{r}_i^H \tag{3.17}$$

The new data $\mathbf{r}_n$ is the filtered received signal vector as defined in (3.16). This expression gives equal weight to each input vector within a sliding window of a constant N vectors. With this scheme however, there needs to be additional work done to update and downdate the R_n matrix. Updating is the process whereby a new input vector is added to the sum, and downdating is where the oldest vector is removed from the sum. Thus the method requires that all N of the most recent input vectors are continually in fast storage.

A perhaps more attractive model is the exponential window model. In this model the covariance matrix is approximated with the following recursive relationship:

$$\mathbf{R}_n = \alpha \mathbf{R}_{n-1} + (1-\alpha)\mathbf{r}_n \mathbf{r}_n^H \tag{3.18}$$

where $\mathbf{R}_n = \mathbf{R}(nT)$, T is the symbol period, and $0 \leq \alpha \leq 1$ is the forgetting factor. Using the forgetting factor to put more or less emphasis on the old data with respect to the new data, the equation is adjustable according to the fading rate. This is the method that was developed for this thesis.

The next section deals with the details of the scheme for iterative eigendecomposition of the autocorrelation matrix. First the basic algorithm will be explained, and then a simplified version of the algorithm will be described. The sections following these will deal with the use of the eigenvalues and eigenvectors of the autocorrelation matrix for detection.

3.3.1 Subspace-tracking Algorithm

The algorithm for the iterative construction and eigendecomposition of the estimated covariance matrix in (3.18) follows [DR90]. It rests on the assumption that the statistics of the channel are slowly varying, and ergodic over a period of $1/(1-\alpha)$.

If the eigenstructure of the previous autocovariance matrix $\mathbf{R}_{n-1}$ is known, from the previous iteration of the algorithm, the equation (3.18) becomes:

$$\begin{aligned} \mathbf{R}_n &= \alpha \mathbf{V}_{n-1} \mathbf{\Lambda}_{n-1} \mathbf{V}_{n-1}^H + (1-\alpha) \mathbf{r}_n \mathbf{r}_n^H \\ &= \mathbf{V}_{n-1} [\alpha \mathbf{\Lambda}_{n-1} + (1-\alpha) \mathbf{x}_n \mathbf{x}_n^H] \mathbf{V}_{n-1}^H \end{aligned} \tag{3.19}$$

where

$$\mathbf{x}_n = \mathbf{V}_{n-1}^H \mathbf{r}_n \tag{3.20}$$

The next step is to multiply the complex vector $\mathbf{x}_n$ by the hermetian of the matrix $\mathbf{G}_n$:

$$\mathbf{G}_n = \begin{bmatrix} \frac{x_1}{|x_1|} & & \mathbf{0} \\ & \frac{x_2}{|x_2|} & \\ & \ddots & \\ \mathbf{0} & & \frac{x_K}{|x_K|} \end{bmatrix} \tag{3.21}$$

The purpose of this step is twofold. First of all it changes $\mathbf{x}_n$ from a complex vector into a real vector, simplifying the decomposition without changing the result. Second, the $\mathbf{G}_n$ matrix now stores the phase information instead of $\mathbf{x}_n$, which is very important to the detection. Now the autocovariance becomes:

$$\mathbf{R}_n = \mathbf{V}_{n-1}\mathbf{G}_n[\alpha\mathbf{\Lambda}_{n-1} + (1-\alpha)\mathbf{q}_n\mathbf{q}_n^T]\mathbf{G}_n^H\mathbf{V}_{n-1}^H \tag{3.22}$$

with

$$\mathbf{q}_n = \mathbf{G}_n^H\mathbf{x}_n \tag{3.23}$$

The terms within brackets in the above expression is now a rank-one matrix added to a diagonal matrix of eigenvalues. The eigenproblem can be deflated, ie, mapped into an equivalent but sparser data matrix that consists mostly of zeroes, by applying the Householder transform [Ste88] to $\mathbf{q}_n$. Since the last $K-D$ eigenvalues are in theory identical, and in practice very similar, we can force the $(K-D)$-dimensional subspace to be spherical. The vector becomes $\mathbf{s}_n = [q_1, \cdots, q_D, (\sum_{i=D+1}^{K} q_i^2)^{\frac{1}{2}}, 0, \cdots, 0]$, with the $(D+1)^{st}$ component being the average of the last $K-D$ components. The transform

is given by:

$$\mathbf{H}_n = \begin{bmatrix} \mathbf{I}_D & \mathbf{0} \\ \mathbf{0} & \mathbf{H}^{(v)}_{K-D} \end{bmatrix} \tag{3.24}$$

where $\mathbf{H}^{(v)}_{K-D}$ is the Householder matrix formed using the last $K-D$ components of $\mathbf{q}_n$.

$$\mathbf{H}^{(v)}_{K-D} = \mathbf{I}_{K-D} - \frac{2\mathbf{e}_n\mathbf{e}_n^T}{\|\mathbf{e}_n\|^2} \tag{3.25}$$

where

$$\mathbf{e}_n = \mathbf{q}_{n,(D+1:K)} - \|\mathbf{q}_{n,(D+1:K)}\| \begin{bmatrix} 1 & 0 & \dots & 0 \end{bmatrix}^T \tag{3.26}$$

In (3.26), all vectors are of length $K-D$; $[\,1\ 0\ \dots\ 0\,]^T$ is a unit vector with only the first component non-zero, and $\mathbf{q}_{n,(D+1:K)}$ represents the last $K-D$ components of $\mathbf{q}_n$.

Since the rank-one matrix $\mathbf{s}_n\mathbf{s}_n^T$ will be of reduced size, the other addend $\mathbf{\Lambda}_{n-1}$ must also be simplified, by averaging the last $K-D$ eigenvalues:

$$\mathbf{D}_{n-1} = \begin{bmatrix} \lambda_{n-1,1} & & & \mathbf{0} \\ & \ddots & & \\ & & \lambda_{n-1,D} & \\ \mathbf{0} & & & \bar{\lambda}_{n-1}\mathbf{I}_{K-D} \end{bmatrix} \tag{3.27}$$

$$\bar{\lambda}_{n-1} = \frac{1}{K-D}\sum_{i=D+1}^{K} \lambda_i. \tag{3.28}$$

Finally,

$$\mathbf{R}_n = \mathbf{V}_{n-1}\mathbf{G}_n\mathbf{H}_n[\alpha\mathbf{D}_{n-1} + (1-\alpha)\mathbf{s}_n\mathbf{s}_n^T]\mathbf{H}_n^T\mathbf{G}_n^H\mathbf{V}_{n-1}^H, \qquad \mathbf{s}_n = \mathbf{H}_n^T\mathbf{q}_n \tag{3.29}$$

where the factoring out of $\mathbf{G}_n$ and $\mathbf{H}_n$ do not affect $\mathbf{D}_{n-1}$ because they are unitary transforms.

Having created this inner matrix $\mathbf{S}_n = \alpha\mathbf{D}_{n-1} + (1-\alpha)\mathbf{s}_n\mathbf{s}_n^T$, there is the matter of finding the eigenvalues and eigenvectors of a small, dense symmetric matrix. There are several ways to do this; in 3.5, two such methods are explored. Once the decomposition $\mathbf{S}_n = \mathbf{U}_n\mathbf{D}_n\mathbf{U}_n^T$ is found, the updated eigenvectors may be determined:

$$\mathbf{V}_n \approx \mathbf{V}_{n-1}\mathbf{G}_n\mathbf{H}_n\mathbf{U}_n \tag{3.30}$$

3.3.2 Simplified Subspace-tracking Algorithm

For detection, D dominant "signal + noise" eigenvalues and eigenvectors are needed, as well as one eigenvalue representing the average power of the noise subspace, and a corresponding eigenvector. After the application of the Householder transform to the K-dimensional vector $\mathbf{q}_n$, the dimension of the core eigenproblem is reduced to $(D+1)$, even though the matrix $\mathbf{S}_n$ is $K \times K$. However, knowing that only the requisite $D+1$ eigenvalues and eigenvectors need to be calculated, the entire algorithm can be simplified even further [Pat96].

At time period n, the dominant D eigenvectors of $\mathbf{V}_{n-1}$ will be used to create the vector $\mathbf{q}_n$.

$$\mathbf{q}_n = \Big[\mathbf{G}_n\Big]_{D\times D}\Big[\quad \mathbf{V}_{n-1}^H \quad\Big]_{D\times K}\left[\mathbf{r}_n\right]_{K\times 1} \tag{3.31}$$

The vector $\mathbf{s}_n$ is identical to $\mathbf{q}_n$ in its first D elements. The $(D+1)^{st}$ element is given by:

$$\mathbf{s}_{n,D+1} = \sqrt{\|\mathbf{r}_n\|^2 - \|\mathbf{q}_{n,1:D}\|^2} \tag{3.32}$$

In other words, the energy in $\mathbf{r}_n$ not contained in $\mathbf{q}_{n,1:D}$ goes into the representative component of the noise subspace.

Using this method, the matrix $\mathbf{U}_n$ becomes $(D+1) \times (D+1)$. Then, from equation (3.30):

$$\begin{aligned}\mathbf{V}_n &\approx \mathbf{V}_{n-1}\mathbf{G}_n\mathbf{H}_n\mathbf{U}_n \\ &= \begin{bmatrix} \uparrow & \uparrow & & \uparrow \\ \mathbf{v}_1 & \mathbf{v}_2 & \cdots & \mathbf{v}_K \\ \downarrow & \downarrow & & \downarrow \end{bmatrix} \begin{bmatrix} \frac{x_1}{|x_1|} & & & \mathbf{0} \\ & \frac{x_2}{|x_2|} & & \\ & & \ddots & \\ \mathbf{0} & & & \frac{x_K}{|x_K|} \end{bmatrix} \begin{bmatrix} \mathbf{I}_D & \mathbf{0} \\ \mathbf{0} & \mathbf{H}^{(v)}_{K-D} \end{bmatrix} \begin{bmatrix} \mathbf{U}_{D+1} & \mathbf{0} \\ \mathbf{0} & \mathbf{I}_{K-D-1} \end{bmatrix}\end{aligned} \tag{3.33}$$

Notice that the first three matrices in the above expression can easily be broken down by column:

$$\mathbf{V}_{n-1}\mathbf{G}_n\mathbf{H}_n = \tilde{\mathbf{V}} = \begin{cases} \begin{bmatrix} \uparrow & \uparrow & & \uparrow \\ \mathbf{v}_1\frac{x_1}{|x_1|} & \mathbf{v}_2\frac{x_2}{|x_2|} & \cdots & \mathbf{v}_D\frac{x_D}{|x_D|} \\ \downarrow & \downarrow & & \downarrow \end{bmatrix} & \text{for columns 1 to } D, \\ \begin{bmatrix} \uparrow & \uparrow & \uparrow \\ \mathbf{v}_{D+1}\frac{x_{D+1}}{|x_{D+1}|} & \cdots & \mathbf{v}_K\frac{x_K}{|x_K|} \\ \downarrow & \downarrow & \downarrow \end{bmatrix} \begin{bmatrix} \\ \mathbf{H}^{(v)}_{K-D} \\ \\ \end{bmatrix} & \text{for columns } D+1 \text{ to } K \end{cases} \tag{3.34}$$

The first D columns above may be calculated fairly easily as shown. Of the rest of the columns, only the $(D+1)^{st}$ column is needed, but as (3.34) illustrates, $\mathbf{v}_{D+1}\ldots\mathbf{v}_K$ and a Householder matrix are required. There is a method of finding $\tilde{\mathbf{v}}_{D+1}$, without the need of the last $K-D$ eigenvectors or a Householder matrix, by forming a projection matrix from the noise subspace and projecting $\mathbf{r}_n$ onto it. Let the noise subspace be spanned by the columns of $\mathbf{V}_{(v)}$ and let the projection matrix for the noise subspace be $\mathcal{P}$. Note that $\mathbf{V}_{(v)}\mathbf{V}^H_{(v)} = \mathbf{I}_K - \mathbf{V}_{(s)}\mathbf{V}^H_{(s)}$, where $\mathbf{V}_{(s)} = [\,\mathbf{v}_1 \cdots \mathbf{v}_D\,]$. The projection matrix is given by $\mathbf{V}_{(v)}$ times the pseudoinverse of $\mathbf{V}_{(v)}$:

$$\begin{aligned} \mathcal{P} &= \mathbf{V}_{(v)}(\mathbf{V}^H_{(v)}\mathbf{V}_{(v)})^{-1}\mathbf{V}^H_{(v)}, \qquad \text{with } \mathbf{V}^H_{(v)}\mathbf{V}_{(v)} = \mathbf{I}_K \\ &= \mathbf{V}_{(v)}\mathbf{V}^H_{(v)} \end{aligned} \tag{3.35}$$

The projection of the vector $\mathbf{r}_n$ onto the noise subspace, $Proj_{\mathbf{V}_{(v)}}(u)$, is $\mathcal{P}\mathbf{r}_n$. Thus

$$\tilde{\mathbf{v}}_{D+1} = \frac{\mathcal{P}\mathbf{r}_n}{\|\mathcal{P}\mathbf{r}_n\|} \tag{3.36}$$

and the eigenvector update becomes:

$$\mathbf{V}_n \approx \begin{bmatrix} \uparrow & \uparrow & & \uparrow \\ \tilde{\mathbf{v}}_1 & \tilde{\mathbf{v}}_2 & \cdots & \tilde{\mathbf{v}_{D+1}} \\ \downarrow & \downarrow & & \downarrow \end{bmatrix} \begin{bmatrix} \mathbf{U}_{D+1} \end{bmatrix} \tag{3.37}$$

Having a smaller $\mathbf{S}_n$ matrix decreases the number of calculations required by the algorithm, since for the most part only D eigenvectors are involved, except for before the update when the noise subspace eigenvector is created.

As an alternative simplification, the complete $K \times K$ matrix $\mathbf{S}_n$ could have been passed to an eigenanalysis routine. This routine could be such that only the largest D eigenvalues and eigenvectors are calculated and stored for further processing, and the $(D+1)^{th}$ eigenvalue/eigenvector pair synthesized as described above. The truncated SVD also suits the purpose. However, this approach precludes the use of the recursive relationship to build $\mathbf{R}_n$, and so would appear more computationally intensive on balance.

3.4 Receiver Structure and Detection

3.4.1 Coherent Detection

Coherent detection may be used to increase link capacity, but the trade-off is that some method of channel estimation is required. With coherent detection of PSK modulated data, the received signal must be adjusted in phase by the amount of phase shift introduced by the channel. The method of obtaining that phase estimate is pilot symbol-assisted channel estimation (PSAM).

As the data is being transmitted, symbols with known phase are introduced into the data stream; these are the pilot symbols. Their function is to enable the channel phase to be approximately estimated at the receiver. The frequency of insertion is significant – for a faster fading channel, more pilot symbols are needed for an accurate estimate. Figure 3.2 is a block diagram of the channel estimation structure at the receiver. The pilot symbols, which are interleaved with data symbols upon arrival, are extracted into the lower branch of the diagram. Because the pilot symbols occur less frequently than the data symbols by a factor of f_P, the samples in the lower branch are upsampled by f_P and interpolated. It is important to note that there are K sample streams being independently filtered and interpolated. The first filter (FIR1) is a linear filter with a bandwidth that matches the fading spectrum, to reduce high-bandwidth noise. The second filter (FIR2) is a lowpass interpolation filter. In the upper branch, the data

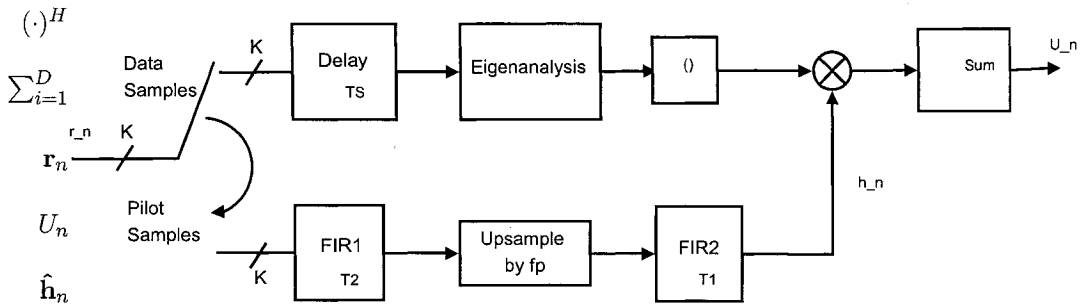

Figure 3.2: Block diagram of receiver for coherent detection.

symbols are subject to a delay equal to that of the lower branch. The eigenanalysis block represents the complete eigendecomposition algorithm including the formation of the autocorrelation matrix $\mathbf{R}_n$.

Once a channel gain and phase estimate has been determined from the pilot symbol stream, a decision variable is constructed. The channel estimate vector represents the individual channel gains and phase shifts for each of the K paths. It is combined as an inner product with each transposed eigenvector, nullifying the phase offset and weighting by the path gain. Each of the D eigenvectors is weighted by the square root of the corresponding eigenvalue.

$$U_n = \Re\left[\sum_{i=1}^{D} \eta_{n,i} \mathbf{v}_{n,i}^H \hat{\mathbf{h}}_n\right] \tag{3.38}$$

Here the variable i indexes the eigenvectors $\mathbf{v}$ at time t_n, $\eta_{n,i} = \sqrt{\lambda_{n,i}}$ where λ_n is the associated eigenvalue, and $\hat{\mathbf{h}}_n$ is the channel estimate vector. This decision variable can be extended to QPSK by including the imaginary part in the computations.

3.4.2 Differential Detection

In the use of differential detection, the channel phase is assumed to remain approximately constant over the symbol period. In conventional differential detection, the received vector is projected onto the previous vector, as in $\mathbf{r}_n\mathbf{r}_{n-1}^H$. The result is the phase difference between them, which is the encoded data. Differential detection has the advantage of not requiring channel estimation, and thus is a popular choice for wireless communications systems where complexity is an issue. There is, however, a 3-dB loss in SNR as compared to coherent detection.

The following decision variable is adapted from that of non-coherent detection of orthogonal waveforms [Pat96].

$$U_n = \Re\left[\sum_{i=1}^{D} \frac{\eta_{n,i} - \eta_{n,D+1}}{\eta_{n,i}} \mathbf{v}_{n-1,i}^H \mathbf{v}_{n,i}\right] \tag{3.39}$$

where

$$\eta_{n,i} = \sqrt{\lambda_{n-1,i}\lambda_{n,i}},\ i = 1, 2, \ldots, D+1 \tag{3.40}$$

The subtraction of the term $\eta_{n,D+1}$ is an attempt to remove the effect of the noise from the i^{th} eigenvalue, which represents the power of the signal and of the noise. The result is a weighted sum of the differences between eigenvectors in consecutive symbol periods.

Note that neither of the decision variables presented (for BPSK or DPSK) contains a transformation of the received signal vector by the eigenvector matrix. The reason

for this omission is that with the subspace tracking algorithm above, $\Re[\mathbf{v}^H\mathbf{r}_n]$ must be always positive or negative, for all eigenvectors. In other words, if (3.41) is not satisfied, the decision variable is meaningless.

$$\text{sgn}(\Re[\mathbf{v}^H\mathbf{r}_n]) = 1(\text{or -1}) \tag{3.41}$$

$$\Im[\mathbf{v}^H\mathbf{r}_n] = 0 \tag{3.42}$$

3.4.3 Rank of the Signal-Noise Subspace

A key point in the development of this algorithm is the determination of the number D of significant signal-noise modes. Up until now in the discussion, it has been assumed simply that D signal eigenvalues and one noise eigenvalue are available. Let us define the integer quantities $r_s(n) < r(n)$ such that $r(n)$ is the total number of signal-noise eigencomponents being tracked at time t_n, and $r_s(n)$ is an estimate of the number D of dominant signal-noise eigencomponents at time t_n. More eigencomponents need to be tracked than are estimated to be part of the signal-noise subspace, so that the rank of the signal subspace can be increased. In this case, one extra signal eigenvalue/eigenvector pair is tracked, so $r(n) = r_s(n)+1$. The noise eigenvalue and eigenvector are in addition to this extra eigenvalue/eigenvector pair.

Before detailing the methods for estimating $r_s(n)$, here is a general approach to increasing and decreasing the working subspace dimension. This subspace dimension

tracking procedure works in concert with the recursive autocorrelation matrix eigenstructure update algorithm described in (3.3.1). The signal eigenvalues are ordered as $\lambda_1 \geq \lambda_2 \geq \cdots \lambda_{r_s(n)} \geq \lambda_{r_s(n)+1}$ and the noise eigenvalue is λ_v.

1. If there has been a subspace dimension increase, append an orthogonal eigenvector $\mathbf{v}_{r_s(n-1)}$ to $\mathbf{V}_{n-1}$, and its corresponding eigenvalue is $\lambda_{n-1,v}$. The orthogonal eigenvector can be found using the projection matrix approach as in (3.36). Now that there are $r(n)$ dominant eigencomponents, perform an eigendecomposition update.

$$\begin{aligned} \mathbf{V}_{n-1} &\rightarrow \mathbf{V}_n \\ \mathbf{\Lambda}_{n-1} &\rightarrow \mathbf{\Lambda}_n \end{aligned} \tag{3.43}$$

2. Estimate the new signal subspace dimension, $r_s(n)$.

3. Let $\mathbf{d}(n) = [\lambda_1, \cdots, \lambda_{r_s(n)}, \lambda_{r_s(n)+1}]$. Three scenarios are possible:

   $r_s(n) = r_s(n-1)$: **no change.** $\mathbf{d}(n)$ contains $r_s(n-1) = r(n-1)-1$ large signal eigenvalues and the last eigenvalue is as small as λ_v

   $r_s(n) < r_s(n-1)$: **dimension decrease.** A number of the smaller elements in $\mathbf{d}(n)$ have approached the level of λ_v. $\mathbf{d}(n)$ must be truncated to size $r_s(n)+1$. $\mathbf{V}_n$ is truncated to the leading $r_s(n)+1$ columns, and $\lambda_{n,v}$ must be recalculated as:

$$\lambda_{n,v} = \frac{1}{r_s(n-1) - r_s(n) + 1} \sum_{i=r_s(n-1)+1}^{r_s(n)+1} \lambda_{n,i} \tag{3.44}$$

$r_s(n) > r_s(n-1)$: **dimension increase.** The last element of $\mathbf{d}(n)$ has become larger than λ_v, resulting in increased rank; $r_s(n) = r_s(n-1) + 1$. The extra eigenvalue is: $\lambda_{r_s(n)+1} = \lambda_v$.

There are many ways of approaching the problem in Step 2, i.e. the subspace dimension detection. One solution is to pick $r_s(n)$ such that the percentage of the total energy in the first $r_s(n)$ modes is greater than or equal to some predetermined threshold, for instance, 95% of the energy. This method will be called the energy criterion method.

The energy criterion method[1] is described algorithmically as follows.

1. Calculate the trace of the autocorrelation matrix

$$Tr = \alpha \left(\sum_{i=1}^{r(n-1)} \lambda_{n-1,i} + \lambda_{n-1,v} \right) + (1-\alpha) \left(\sum_{i=1}^{K} \mathbf{r}_{n,i} \mathbf{r}_{n,i}^H \right) \tag{3.45}$$

2. Test whether the previous dimension estimate, $r_s(n-1)$, contains a sufficient proportion of the currently available energy

$$\left(\sum_{i=1}^{r_s(n-1)} \lambda_{n,i} \right) \geq 0.95 \times Tr \tag{3.46}$$

[1] An interesting variant of the energy criterion method was proposed in [KY96]. The authors suggest that the subspace dimension be determined by the number of eigenvalues greater than a certain tolerance $T(n) = \phi\sqrt{\lambda_{n,D+1}}$, where $\phi > 1$ is a thresholding factor based on an optimality criterion that depends on α,$r_s(n)$,D, and the SNR.

- If the test is positive, then $r_s(n-1)$ is an acceptable estimate, or is an overestimate of the current signal+noise subspace dimension: then set

$$r_s(n) = \min_i \left\{ \sum_{i=1}^{r_s(n-1)} \lambda_{n,i} \geq 0.95 \times Tr \right\} \tag{3.47}$$

- Otherwise, then $r_s(n-1)$ is an underestimate of the current signal+noise subspace dimension. Thus set $r_s(n) = r_s(n-1) + 1$.

This method of dimension detection might work well with the Lanczos algorithm [LT94] for the eigendecomposition update. The Lanczos method, which is described in the next section, computes one Ritz value and one Ritz vector per iteration. The Ritz pair is the best estimate of the eigenvalue/eigenvector pair given the number of iterations performed. At each iteration of the Lanczos method, it is checked whether the sum of the Ritz values exceeds the threshold, $0.95 \times Tr$. Then $r_s(n)$ becomes the minimum number of Ritz values that satisfies the criteria.

Another approach to track the subspace dimension is to use an information criterion [WK85] to determine $r_s(n)$. This class of methods depends on the fact that while the noise eigenvalues of the estimated autocorrelation matrix will not all be the same value, as they would if it were an ideal autocorrelation matrix, they will all be clustered in a small region. The following statistic detects whether the arithmetic means and

geometric means of $\lambda_{d+1}, \cdots, \lambda_K$ are close to each other.

$$L(d) = N(K-d) \ln \left[\frac{\frac{1}{K-d} \sum_{i=d+1}^{K} \lambda_{n,i}}{\left(\prod_{i=d+1}^{K} \lambda_{n,i} \right)^{1/(K-d)}} \right], \quad d = 0, 1, 2, \ldots, K \tag{3.48}$$

where d is an index over the possible dimensions, K is the largest dimension under consideration, and N is the number of input vectors involved in the formation of the autocorrelation matrix. The statistic $L(d)$ is called a likelihood ratio. As d approaches D, there is a change in the behaviour of the likelihood ratio that indicates the best estimate has been found. The AIC (Akaike Information Criterion) and MDL (Minimum Description Length) criterion are based on the likelihood ratio. The dimension $r_s(n)$ is determined by finding the minimum of:

$$AIC(d) = L(d) + d(2K - d) \tag{3.49}$$

$$MDL(d) = L(d) + \frac{1}{2} d(2K - d) \log N \tag{3.50}$$

Thus the second dimension detection algorithm is called the information criterion method. The procedure is as follows:

1. Calculate the likelihood function $L(d)$. Note that the last $K - r(n-1)$ eigenvalues have been averaged and are assumed to be equal, making $AIC(d)$ and $MDL(d)$ strictly increasing functions in d. Thus we only need to calculate $AIC(d)$ or

$MDL(d)$ for $d \leq r(n-1)$.

$$L(d) = N(r(n-1)+1-d) \ln \left[\frac{\frac{1}{r(n-1)+1-d} \sum_{i=d+1}^{r(n-1)+1} \lambda_{n,i}}{\left(\prod_{i=d+1}^{r(n-1)+1} \lambda_{n,i} \right)^{1/(r(n-1)+1-d)}} \right], \quad d = 0, 1, 2, \ldots, r(n-1) \tag{3.51}$$

where the number of significant vectors can be approximated with the expression $N = 1/(1-\alpha)$ [DR90].

2. Find the estimated dimension using the MDL or AIC criterion:

$$r_{s,AIC}(n) = \arg \min_d \{L(d) + d(2r(n) + 2 - d)\} \tag{3.52}$$

$$r_{s,MDL}(n) = \arg \min_d \{L(d) + \frac{d}{2}(2r(n) + 2 - d) \ln(N)\} \tag{3.53}$$

In Chapter 4, simulation results will be presented that compare the effectiveness of the two dimension detection algorithms. In the next section, the details of two eigendecomposition routines, which are the foundation of the eigenanalysis receiver, are described.

3.5 Eigenanalysis

At the core of the detection algorithm lies the problem of rapidly finding the eigenvalues of an $\mathsf{N} \times \mathsf{N}$, real symmetric matrix. With the exception of the transient case at the startup of the algorithm, the rank of the matrix is N, which implies there are

N non-zero eigenvalues. The non-zero eigenvalues are always nondegenerate, meaning there are no multiples; each one is distinct.

The methods visited here will be: the QR algorithm and the Lanczos method. The QR algorithm is part of the class of block algorithms because it operates directly on the matrix itself using matrix transformation. The advantage of block algorithms is their speed. Iterative algorithms, such as the Lanczos method, are useful in this case because of their flexibility; not all the eigenvalues need to be found but perhaps only D of the largest.

For both methods of eigendecomposition considered here, an initial simplification of the input matrix should be done, namely, to reduce the matrix to tridiagonal form. The reduction enhances the speed of the eigendecomposition. It is done by applying a series of plane rotations, such as Givens or Householder transformations, to the matrix designed to eliminate all elements except those on the diagonal, subdiagonal and superdiagonal. These methods produce the same result, but the Givens method requires approximately twice the elementary operations that the Householder method does, accounting for the creation of the transformation matrix itself and for the zeroing out of the entire column [W. 02]. For this reason, the Householder transformation method is chosen.

3.5.1 QR Algorithm

The QR algorithm is based upon the QR factorization $\mathsf{A} = \mathsf{QR}$ where Q is a unitary matrix and R is upper triangular. Noting that $\mathsf{Q}_k\mathsf{Q}_k' = \mathsf{I}$, observe that:

$$\mathsf{A} = \mathsf{QR} \tag{3.54}$$

$$\mathsf{Q}'\mathsf{AQ} = \mathsf{Q}'(\mathsf{QR})\mathsf{Q} = \mathsf{RQ} \tag{3.55}$$

In its simplest form, the QR algorithm involves reducing a matrix to diagonal form by performing series of unitary transformations $\mathsf{Q}_k'\mathsf{A}_k\mathsf{Q}_k$:

For $k = 0, 1, 2...$

$$\mathsf{A}_k = \mathsf{Q}_k\mathsf{R}_k \tag{3.56}$$

$$\begin{aligned} \mathsf{A}_{k+1} &= \mathsf{R}_k\mathsf{Q}_k \\ &= \mathsf{Q}_k'\mathsf{A}_k\mathsf{Q}_k \\ &= (\mathsf{Q}_{k-1}\ldots\mathsf{Q}_0)'\mathsf{A}(\mathsf{Q}_0\ldots\mathsf{Q}_{k-1}) \end{aligned} \tag{3.57}$$

Eventually A_{k+1} will become diagonal to working precision, and the values on the diagonal will be the eigenvalues. The columns of Q_k, the accumulated set of unitary transformations $\mathsf{Q}_{k-1}\ldots\mathsf{Q}_1\mathsf{Q}_0$, will be the eigenvectors. Because the Q_k are similarity transformations, they do not change the eigenvalues of A.

Each of the unitary transformations Q_k is an accumulation of Givens rotations [T. 00]. These rotations eliminate all the subdiagonal elements in the tridiagonal matrix.

$$\mathsf{Q}_k^T = \mathsf{P}_{12}^{(k)} \cdot \mathsf{P}_{23}^{(k)} \cdots \mathsf{P}_{n-1,n}^{(k)} \tag{3.58}$$

where $\mathsf{P}_{n-1,n}^{(k)}$ is designed to eliminate element $\mathsf{a}_{n-1,n}$.

Performed exactly as described above, the QR algorithm is not particularly fast; a superdiagonal element converges to zero as $\mathsf{a}_{ij}^{(k)} \backsim (\frac{\lambda_i}{\lambda_j})^k$. The element will always converge since $\lambda_i < \lambda_j$, but it can be slow if λ_i is close to λ_j. It is better to apply a shift, s_k, to A at each iteration. The addition of a shift causes the eigenvalues to be changed by s_k, which can hasten convergence if the shift is appropriately chosen, while leaving the eigenvectors unaffected. In the shifted QR algorithm, the QR factorization is performed on:

$$\mathsf{A}_k - \mathsf{s}_k\mathsf{I} = \mathsf{Q}_k\mathsf{R}_k \tag{3.59}$$

and then A_{k+1} is formed as:

$$\mathsf{A}_{k+1} = \mathsf{R}_k\mathsf{Q}_k + \mathsf{s}_k\mathsf{I} \tag{3.60}$$

The shift is newly selected at each step, and the convergence is now as $\frac{\lambda_i - \mathsf{s}_k}{\lambda_j - \mathsf{s}_k}$. There are various shifting strategies. The Wilkinson shift involves computing the eigenvalues of a 2×2 matrix encasing the next diagonal element to converge ($\mathsf{a}_{m,m}$), and then using the eigenvalue closest to $\mathsf{a}_{m,m}$. A simpler strategy, the Rayleigh shift, uses the diagonal

Table 3.1: Computational Complexity of the QR Algorithm

Item	**Number of operations**
Reduction to tridiagonal form	$4N^3/3$
QR algorithm†	$3N^3$

† Assuming an average number of QR iterations per eigenvalue of 1.3-1.6. Eigenvectors are calculated as well as eigenvalues.

element $a_{m,m}$ itself as the shift. [LT94] shows numerically the convergence advantage of using the two shift types mentioned.

One further refinement should be noted; the algorithm can be made more accurate for small eigenvalues with the use of implicit shifts. Instead of subtracting a large s_k from the diagonal elements of A, which can cause a loss of accuracy, the shift is incorporated into the formation of the plane rotation.

The routines used to implement the above algorithm are "tred" (reduction to triangular form) and "tqli" (tridiagonal QL with implicit shifts) from [W. 02]. The mathematically equivalent QL algorithm is used instead of QR, which is based on the lower triangular factorization $A = QL$ instead of the upper triangular factorization.

3.5.2 Lanczos Algorithm

The Lanczos method for finding the eigenvalues of a symmetric matrix has been particularly useful for sparse matrices. This is due to the fact that only two vectors at a time need to be kept in fast storage. It generates a small tridiagonal matrix T_j whose eigenvalues approximate the eigenvalues of the larger input matrix. The algorithm can be stopped at any time, for instance, when a sufficient number of eigenvalues have been calculated. Since the detection algorithm requires only that a subset of the largest eigenvalues and eigenvectors are found, this method suits the purpose.

The Lanczos method is based upon the following theorem:

Theorem 1. *Let* A *be Hermetian, and assume that* Q *is a unitary matrix such that* $\mathsf{Q}^H\mathsf{A}\mathsf{Q} = \mathsf{H}$, *where* H *is real tridiagonal with positive off-diagonal elements. Then* H *and* $\mathsf{Q} = (\mathsf{q}_1, \mathsf{q}_2, \cdots, \mathsf{q}_n)$ *are uniquely determined by* A *and* q_1.

The method uses a three-term recurrence relationship between the basis vectors q_j to build the next vector in the expansion. The starting vector is usually randomly-generated, but a unit vector with components of equal magnitude is also a good choice[2].

[2]The starting vector is very important to the successful completion of the Lanczos method. If the starting vector has a component which is zero, it may inhibit the method from finding Lanczos vectors that form a basis for the subspace spanned by the input matrix.

In exact arithmetic the relationship is:

$$\mathsf{A} \cdot \mathsf{Q}_j = \mathsf{Q}_j \cdot \mathsf{T}_j + \gamma_j \cdot \mathsf{v}j + 1 \cdot \mathsf{e}_{j+1}^T \tag{3.61}$$

where Q_j consists of the first j columns of Q, $\mathsf{Q}_j^H \mathsf{Q}_j = \mathsf{I}$, e_{j+1} is the $(j+1)^{st}$ canonical basis vector. T_j is defined as:

$$\mathsf{T}_j = \begin{bmatrix} \alpha_1 & \beta_1 & & & \\ \beta_1 & \alpha_2 & \beta_2 & & \\ & \ddots & \ddots & \ddots & \\ & & \ddots & \ddots & \beta_{j-1} \\ & & & \beta_{j-1} & \alpha_j \end{bmatrix} \tag{3.62}$$

with $\alpha_i = \mathsf{q}_i^H \cdot \mathsf{A} \cdot \mathsf{q}_i$ and $\beta_i = \|\mathsf{r}_i\|$. The vectors q_j are called the Lanczos vectors. At each step, an additional row and column are added to T_j and the relationship $\mathsf{Q}_j^H \cdot \mathsf{A} \cdot \mathsf{Q}_j = T_j$ holds.

The eigenvalues τ_j of T_j are called the Ritz values,

$$\mathsf{T}_j \cdot \mathsf{g}_i^{(j)} = \tau_i^{(j)} \cdot \mathsf{g}_i^{(j)}, i = 1, 2, ..., j \tag{3.63}$$

and the Ritz vectors are as follows:

$$\mathsf{y}_i^{(j)} = \mathsf{Q}_j \cdot \mathsf{g}_i^{(j)}, i = 1, 2, ..., j \tag{3.64}$$

The Ritz values and vectors are the best approximations to the eigenvalues and eigenvectors of A, using the information in Q_j. Obtaining the final (converged) Ritz values

and vectors is the goal of the algorithm.

The algorithm itself can be derived from the vector form of Equation (3.61). The formula for the residual at each step is:

$$\mathsf{r}_j = \beta_j \cdot \mathsf{q}_{j+1} = \mathsf{A} \cdot \mathsf{q}_j - \alpha_j \cdot \mathsf{q}_j - \beta_{j-1} \cdot \mathsf{q}_{j-1} \tag{3.65}$$

from which the algorithm for finding T_j and the Lanczos vectors can be deduced.

The Lanczos Procedure $\mathsf{q}_0 = 0$. Select q_1 such that $\|\mathsf{q}_1\|_2 = 1$

For $j = 1, 2, ...,$ until enough Ritz pairs are converged, or $\beta_j = 0$

1. $\mathsf{z}_j = \mathsf{A} \cdot \mathsf{q}_j - \beta \cdot \mathsf{q}_{j-1}$
2. $\alpha_j = < \mathsf{z}_j, \mathsf{q}_j >$
3. $\mathsf{z}_j = \mathsf{z}_j - \alpha_j \cdot \mathsf{q}_j$
4. Reorthogonalize: For $k = j : -1 : 1$ $(\mathsf{z}_j = \mathsf{z}_j - \mathsf{q}_k \cdot \mathsf{q}_k^T \cdot \mathsf{z}_j)$
5. $\beta_j = \|\mathsf{z}_j\|_2$
6. $\mathsf{q}_{j+1} = \frac{\mathsf{z}_j}{\beta_j}$

The end of the recursion occurs when the desired number of Ritz values and vectors have been obtained. It is not the case that a newly created Lanczos vector implies a

converged Ritz vector. Usually[3], a couple of iterations more will be necessary to cause the Ritz vector to converge. The following criterion may be used to determine whether a given Ritz pair has converged:

Theorem 2. *The norm of the residual* $\mathsf{r}_i^{(j)} = \mathsf{A} \cdot \mathsf{y}_i^{(j)} - \tau_i^{(j)} \cdot \mathsf{y}_i^{(j)}$ *is equal to* $\beta_j |\mathsf{e}_j^T \cdot \mathsf{g}_i^{(j)}|$, *the last component of the Ritz vector multiplied by* β_j.

However, for our purposes, the Lanczos procedure is complete when any of the following occurs:

- a complete orthogonal basis for the subspace spanned by A has been found (indicated by β_j going to zero)[4],
- the algorithm runs to the maximum N iterations, or
- the number of Ritz values found is deemed sufficient.

A sufficient number of Ritz values is the number which meets the energy criterion set out in the rank determination algorithm. It is convenient to call a QR routine at the end of a Lanczos iteration to quickly find the eigenvalues of the matrix T_j, without

[3] An heuristic can be used: if r Ritz values are required, perform $j = r + 2$ iterations of the Lanczos algorithm; the extra two iterations ensure that the Ritz values are reasonably accurate.

[4] This condition can occur if the matrix A has a rank less than the full size of the matrix, as is the case on startup of the detection algorithm. The covariance matrix needs several rank-one updates to achieve full rank.

accumulating the eigenvectors. This routine can be part of the rank-estimation test. Then, when the required number of Ritz values are obtained, the iterations cease and the Ritz vectors may be calculated.

When using exact arithmetic, the method produces orthogonal Lanczos vectors; with floating point arithmetic, orthogonality problems arise. After a small β_{ij} has been computed, the Lanczos procedure may produce copies of previous Ritz vector, due to the fact that the new Lanczos vectors could have large components in the direction of previous Ritz vectors. Some form of reorthogonalization must be added between each Lanczos step, to avoid this pitfall. For the implementation used in the detector, a complete reorthogonalization was performed at each step: the new Lanczos vector was orthogonalized with each vector that came before it. A final orthogonalization must be performed on the Ritz vectors after they are found, as well as a normalization.

3.6 Computational Cost of Detection Algorithm

The eigendecomposition itself is $O(r^2N^2)$ for the Lanczos algorithm, and $O(r^3)$ for the QR algorithm. It is difficult to say which would be more expensive computationally, since $r < N$. The total computational cost of the detection algorithm is dependent not only on the method of eigenanalysis used, but also on the cost of the eigenstructure update, and the construction of the decision variable. Many of the operations must be

Table 3.2: Computational Complexity of the Lanczos Method

Item	**Number of Mults**	**Number of Adds**
$z_j = A \cdot q_j - \beta \cdot q_{j-1}$	$r(N^2 + N)$	$r(N^2 + 1)$
$\alpha_j =< z_j, q_j >$	rN	$r(N-1)$
$z_j = z_j - \alpha_j \cdot q_j$	rN	$r(N-1)$
Reorthogonalization	$(r^2 + r)(N^2)$	$\frac{r^2+r}{2}(N^2 - 1)$
$\beta_j = \|z_j\|_2$	rN	$r(N-1)$
$q_{j+1} = \frac{z_j}{\beta_j}$	rN	–
Calculate Ritz values T_j	$30rN^2$	–
Calculate Ritz vectors $y_i^{(j)}$	rN	$N(r-1)$
Orthogonalize Ritz vectors	$2N^2$	$N^2 - 1$
Normalize Ritz vectors	rN	$r(N-1)$
Total	$(r^2 + 32r + 2)N^2 + 7rN$	$(r^2/2 + 3r/2 + 1)N^2 + 5rN$

r is the average dimension of the signal-noise subspace, or equivalently, the average number of Lanczos iterations. N is the size of the input vector $\mathbf{r}_n$

done in complex arithmetic, and so are doubly costly with respect to the eigenanalysis, which is done with real numbers.

After each iteration, all eigenvectors must be re-orthogonalized to avoid the gradual loss of orthogonality that would result from the recursive update. To do a complete Gram-Schmidt orthogonalization [T. 00] would be too expensive, so it has been determined that by simply normalizing the vectors at every iteration, an acceptable level of orthogonality is maintained [DR90]. However, a full Gram-Schmidt must be done when creating the projection vector $\mathcal{P}$, since this vector must be orthogonal to all previous eigenvectors. This is the single most costly part of the eigenstructure update. Overall, the eigenstructure update complexity is on the order of $(r+1)N^2$. The formation of the decision variable adds another Nr complex multiplications.

Table 3.3: Computational Complexity of the Eigenstructure Update

Item	Complex Mults	Complex Adds	Real Mults	Real Adds
$\mathbf{x}_n$	$(r+1)N$	$(r+1)(N-1)$	–	–
$\mathbf{G}_n$	$(r+1)$	–	$2(r+1)$	–
$\mathbf{q}_n$	$(r+1)+N$	–	$r+1$	$2r+N-1$
$\tilde{\mathbf{V}}(1:\mathbf{D})_n$	$(r+1)N$	$(r+1)N$	–	–
$\mathcal{P}$	$(r+1)N^2$	rN^2	–	–
$\tilde{\mathbf{V}}(\mathbf{D}+1)_n$	N^2+N	N^2	$2N$	$2(N-1)$
$\mathbf{S}_n$	$3(r+1)^2$	$(r+1)^2$	–	–
$\mathbf{V}_n$	$N(r+2)^2$	$N(r+1)(r+2)$	–	–
Normalizing $\mathbf{V}_n$	$N(r+1)+N$	$(N-1)(r+1)$	–	–
Total	$O((r+1)N^2)$	$O(rN^2)$	$O(N)$	$O(N)$

r is the average dimension of the signal-noise subspace. N is the size of the input vector $\mathbf{r}_n$

Table 3.4: Computational Complexity of the Decision Variable

Item	Complex Mults	Complex Adds	Real Mults	Real Adds	Functions
$\eta_{n,i}$	–	–	$r+2$	–	$sqrt$
U_n	Nr	–	$2r$	$2r+2N$	–
AIC†	Nr	–	$r+5$	$r+6$	ln, pow

† (Information Criterion Method only). r is the average dimension of the signal-noise subspace. N is the size of the input vector $\mathbf{r}_n$

3.7 Conclusion

In this chapter, a spherical subspace tracker with adaptive rank for detection of PSK signals has been described. The method of recursive update of the autocorrelation matrix eigenstructure was outlined, and a simplified but equivalent version was given. Two methods were outlined for the eigendecomposition; the Lanczos method, and the QR algorithm, and their relative complexity was discussed. Also, two different methods have been proposed for implementing the adaptive rank-determination; the energy criterion method for use with the Lanczos method, and the information criterion method for use with the QR method. In the next chapter, results of simulations of both detectors will be given, for both types of rank-determination method, and for various channels.

Chapter 4

Simulation Results

4.1 Introduction

The detection algorithms defined in the previous chapter are designed to carry a binary signal over channels exhibiting moderate Rayleigh and Rician fading, with or without correlation between paths. It will now be seen how the performance of these algorithms compares to traditional forms of detection, under typical channel conditions. There are many ways of simulating a wireless link; three different methods are used. Briefly, these methods are: classical Doppler filtering using path gains and delays as given by COST-207 and COST-259 models, classical Doppler filtering of orthogonal signal components and multiplication by orthogonal gains, and filtering using measured channel impulse response data. Each of these methods is further described in Appendix B.

For the algorithms to be deemed useful, they need to have not only good performance but fast execution on a digital signal processor. The algorithms have been downloaded to a floating-point DSP, the TI TMS320C6701, and profiled. These results will be presented in the latter half of the chapter.

Before examining the results, it is instructive to first look at an example of the performance of the optimal coherent eigenanalysis-based receiver. In the derivation of this theoretical receiver, it is assumed that the signal ($\mathbf{P}\mathbf{a}_n$) and noise ($\boldsymbol{\upsilon}_n$) parts of $\mathbf{r}_n$ may be separated.

The eigendecomposition of $\mathbf{R}_s$ is known.

$$\mathbf{R}_s = E\left[\mathbf{P}\mathbf{a}_n\mathbf{a}_n^H\mathbf{P}^H\right] = \mathbf{P}\mathbf{R}_a\mathbf{P}^T = \mathbf{V}_s\boldsymbol{\Gamma}_s\mathbf{V}_s^H \tag{4.1}$$

where $\mathbf{P}$ is the combined response of the transmit and receive spreading filters, and $\mathbf{a}_n$ are the path gains corresponding to each peak in $\mathbf{P}$. Each of the eigenvectors in $\mathbf{V}_s$ can be seen as a filter matched to one orthogonal component in the signal part of $\mathbf{r}_n$. Let $\tilde{\mathbf{r}}_n$ represent the new vector after the transformation:

$$\tilde{\mathbf{r}}_n = \mathbf{V}_s^H\mathbf{r}_n \tag{4.2}$$

$$= b_n\mathbf{V}_s^H\mathbf{P}\mathbf{a}_n + \mathbf{V}_s^H\upsilon_n \tag{4.3}$$

$$= b_n\mathbf{g}_n + \mathbf{V}_s^H\upsilon_n \tag{4.4}$$

where $\mathbf{g}_n$ are the orthogonal path gains. By this operation, the signal part of $\mathbf{r}_n$ has

been decorrelated[1]; it remains now to find an appropriate combining method for the $\mathbf{g}_n$.

Let $\mathbf{y}_n$ be the weighting vector, such that the optimal decision variable is:

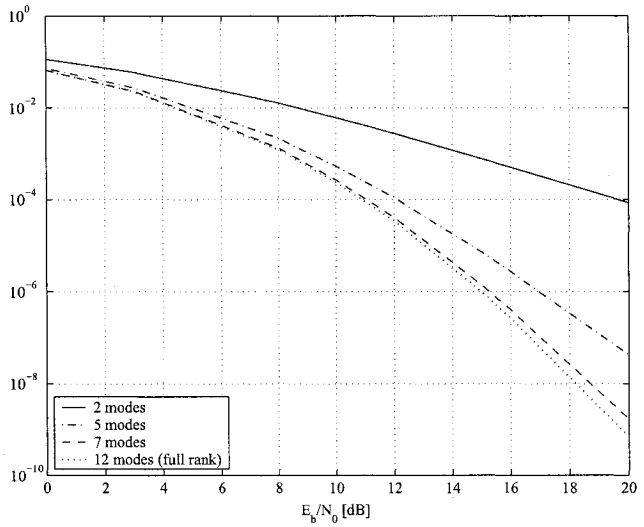

Figure 4.1: Performance of optimal eigenanalysis detector in the presence of AWGN

$$U_n = \mathbf{y}_n^H \tilde{\mathbf{r}}_n \tag{4.5}$$

By maximizing the instantaneous signal to noise ratio of U_n, it can be shown [SW94] that the vector required is $\mathbf{X}^{-1}$:

$$y_n = \mathbf{X}^{-1}\mathbf{g}_n = \mathbf{V}_s^H \mathbf{R}_v^{-1} \mathbf{V}_s \tag{4.6}$$

which completes the formation of the optimal decision variable. Referring to Figure 4.1,

[1]In fact, it was not strictly necessary to do this, since when perfect knowledge of the complex gains $\mathbf{a}_n$ is assumed there is no advantage in terms of performance to applying the decorrelating filters.

one can observe that each additional mode used in the formation of the decision variable decreases the probability of error. Now it will be seen how the addition of more modes affects performance when our eigenvectors are not exact but are estimates.

4.2 Results for GSM Channels

First some results will be shown for a simple form of the eigenanalysis-based detector, in which a fixed number **D** of eigenpairs are provided at decision time. Though the actual dimension may be determined to be less than that fixed number, the algorithm starts again at the next symbol with a full complement of **D** eigenvectors and eigenvalues. This algorithm will be called the fixed-D detector. The difference between the fixed-D form of the detector and the algorithm described in Chapter 3, is that the algorithm described in Chapter 3 permits the addition of one eigenpair or the removal of several eigenpairs from the eigenstructure update. For a table of the naming convention used for the graphs, see Table 4.1.

The system was simulated 4 times with different random seeds for the multipath simulator and PSK data generator, and the results averaged to form the composite result. Each data point is the result of simulating at least (but not limited to) 50 errors, or in the case of the higher-SNR data points, 10^5 symbols, in which case the number of errors was at least 5.

Table 4.1: Detection scheme naming convention

Name	Description	Decision Variable
Eigen,$D = 2$	Eigenanalysis detection, 2 modes maximum, information criterion.	Eqn 3.39 or Eqn 3.38
Eigen,$D = 5$	Eigenanalysis detection, 5 modes maximum, information criterion.	Eqn 3.39 or Eqn 3.38
CCD	Conventional coherent detection.	$U_n = \left[\mathbf{r}_n^H \hat{\mathbf{h}}_n\right]$
EigenIC	Eigenanalysis detection, variable D, information criterion.	Eqn 3.39
EigenEC	Eigenanalysis detection, variable D, energy criterion.	Eqn 3.39
DD	Conventional differential detection.	$U_n = \left[\mathbf{r}_n^H \mathbf{r}_{n-1}\right]$

Considering first the fixed-D algorithm, the effectiveness of the detector is examined for different types of modulation: DPSK, BPSK, and QPSK. Figure 4.2 shows the bit error rate performance for a BPSK receiver where the channel estimation is done by Pilot Symbol Assisted Modulation (PSAM). Results for three different fading rates are given, where the fading rate is specified using the expression $f_D T$, which is the maximum Doppler frequency normalized by the symbol rate. Note that different alpha values are preferable at different fading rates (when the fading is faster the window of observation can be smaller). The channel model is the GSM Typical Urban (TU) COST-207 model, which comprises 12 paths of varying strength, with a delay spread of about $0.7\mu s$.

From Figures 4.2 and 4.3 it is apparent that the performance of the coherent receiver is quite susceptible to fading. The positive effects of diversity on the probability of error are not strong enough to produce an exponential curve at higher fading rates. The channel estimation method used (PSAM) did not seem to perform well under the simulated fading channel conditions. In the slow fading case ($f_D T = 0.01$) with BPSK modulation, conventional detection performed the best, followed by the eigenanalysis detector using $D = 2$ modes. At high SNR, the detector using $D = 5$ had more bit errors, probably because a larger number of modes went into the creation of the decision variable than was optimal. The behaviour of the AIC criterion is different depending on the maximum number of modes D.

Comparing the two eigenanalysis algorithms, at slow fading the scheme using fewer modes is still superior, while as the fading begins to dominate, the two algorithms seem to behave almost identically. It is interesting to note that the eigenanalysis algorithms outperform the conventional QPSK at faster fading rates, though all algorithms suffer

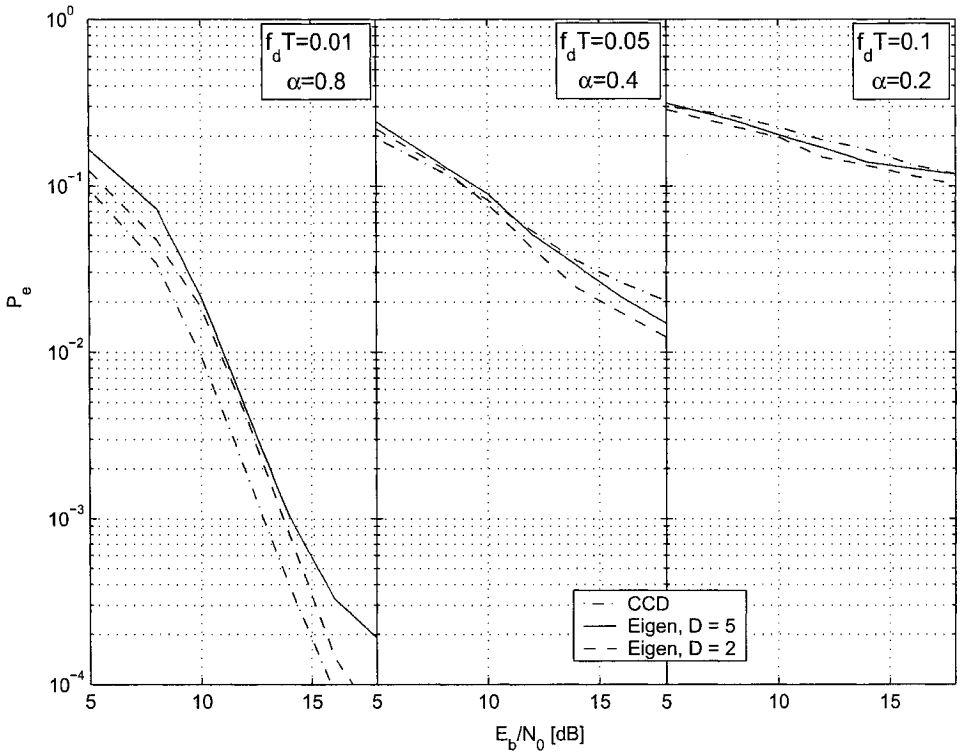

Figure 4.2: Performance of fixed-D algorithms with COST-207 channel, for BPSK modulation

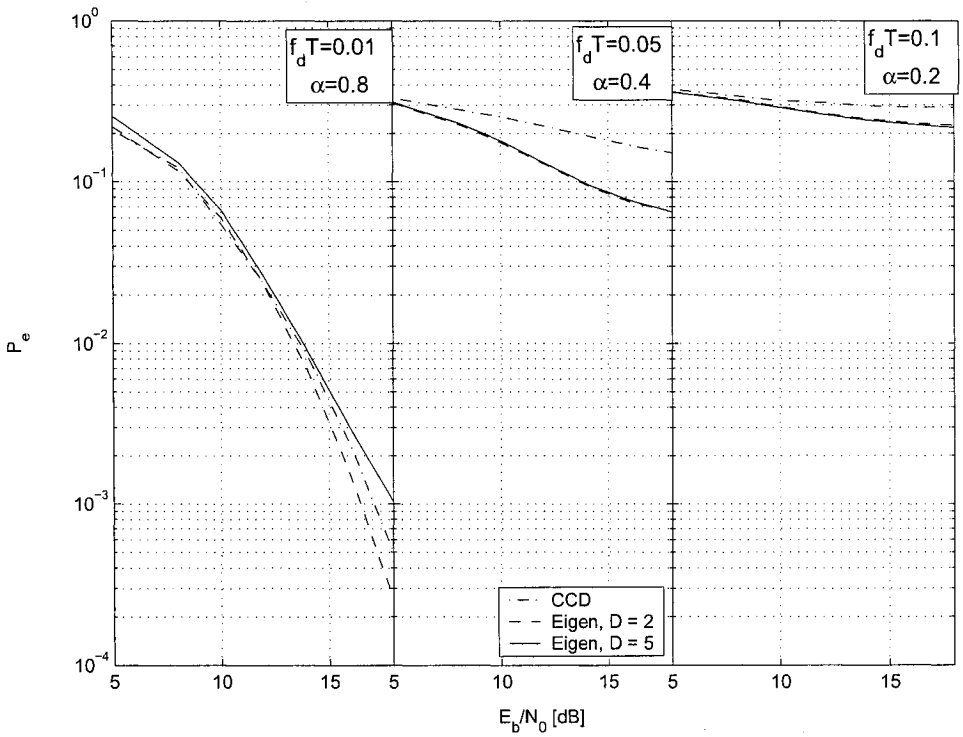

Figure 4.3: Performance of fixed-D algorithms with COST-207 channel, for QPSK modulation

greatly with an increase in f_DT.

The DPSK implementation of the fixed-D algorithm, whose performance is shown in Figure 4.4, better illustrates the potential of the eigenanalysis approach. With slow fading, the eigenanalysis detectors ($D = 2$ and $D = 5$), perform better than the con-

ventional detector, at least up to an SNR of about 18 dB. As the fading rate increases, the eigenanalysis detectors perform very much like the conventional detector, with just a little more sensitivity to fading at high SNR.

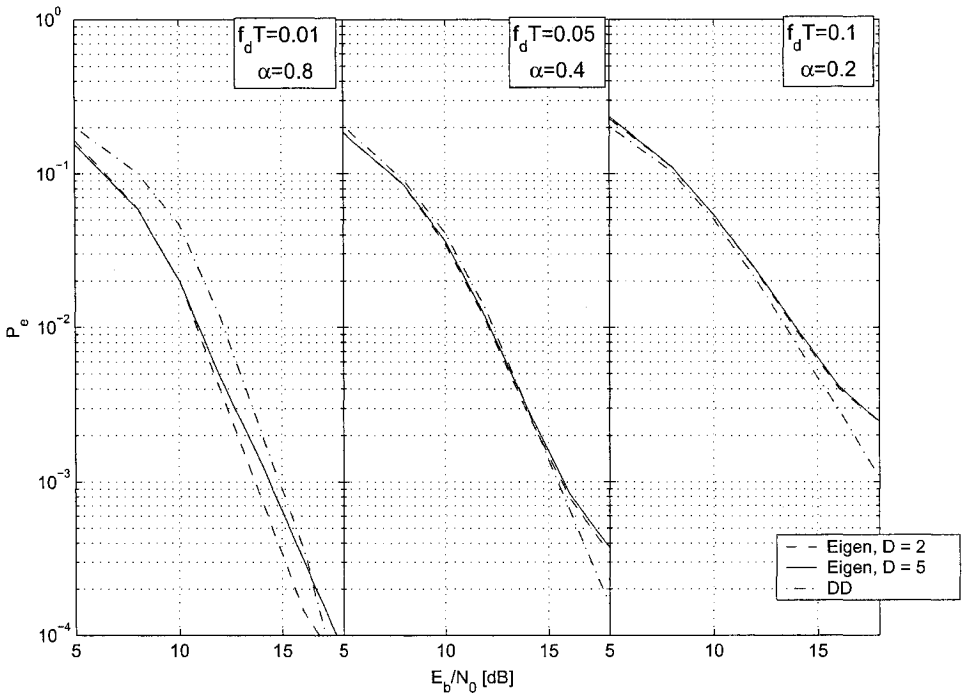

Figure 4.4: Performance of fixed-D algorithms with COST-207 channel, for DPSK modulation

From the above graphs, it would seem that more dimensions does not mean better performance: in fact, the smaller D-value produced better results most of the time. The reason for this may be that the simulated channel has an effective orthogonal dimension which is small, so by restricting the range of dimensionality to 2, the dimension is more accurately estimated.

In Chapter 3, two methods of estimating and autonomously increasing or decreasing the parameter D were presented. The next graphs show performance results of these schemes, where the data is modulated using DSPK. To illustrate the effect of different channel conditions, results are also plotted for COST-259 typical urban (TU) channel, which has a higher number of paths and a longer delay spread than the COST-207 TU channel. Both of these channels are described in Appendix B.

It is notable from Figures 4.5 and 4.6 that the energy criterion method does not perform as well as the information criterion method. One possible reason for this is that the energy criterion method tends to overestimate the signal-noise subspace dimension. For all the simulations involving the energy criterion method, the energy threshold was set to 80%, since a larger threshold introduced too many noise eigenvectors and drastically increased the probability of error.

As the fading rate increases, the energy criterion method shows less deterioration when simulated with the COST-259 channel than with the COST-207 channel. This behaviour may be due to the greater number of modes in the COST-259 channel, so that when the channel is in a fade, the algorithm may have a greater diversity of modes

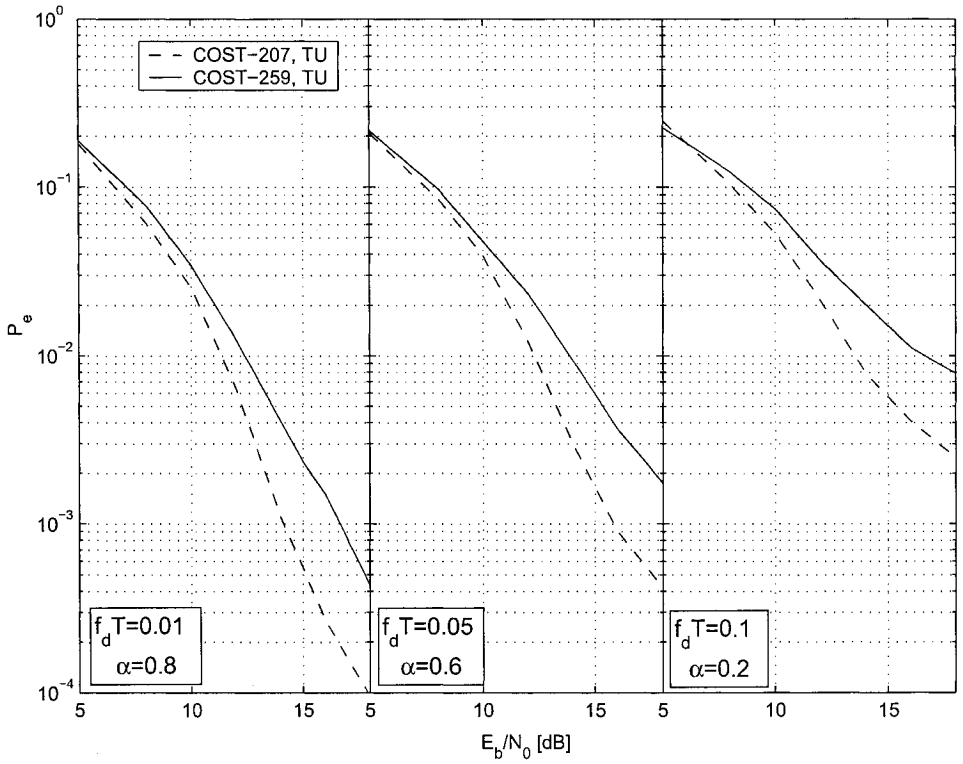

Figure 4.5: Performance of EigenIC dimension estimation scheme with both COST-207 and COST-259 typical urban channels

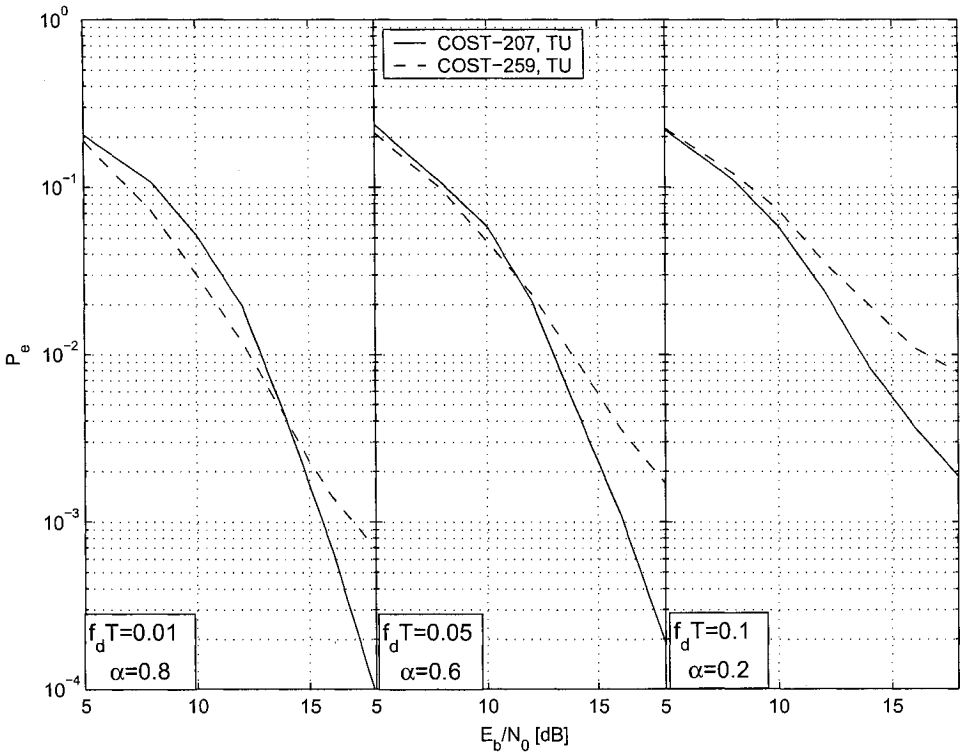

Figure 4.6: Performance of EigenEC dimension estimation scheme with both COST-207 and COST-259 typical urban channels

to fall back on than in the COST-207 channel.

The GSM channels introduce a high degree of overlap between paths, contributing to some inter-path correlation, but there was no correlation explicitly introduced between

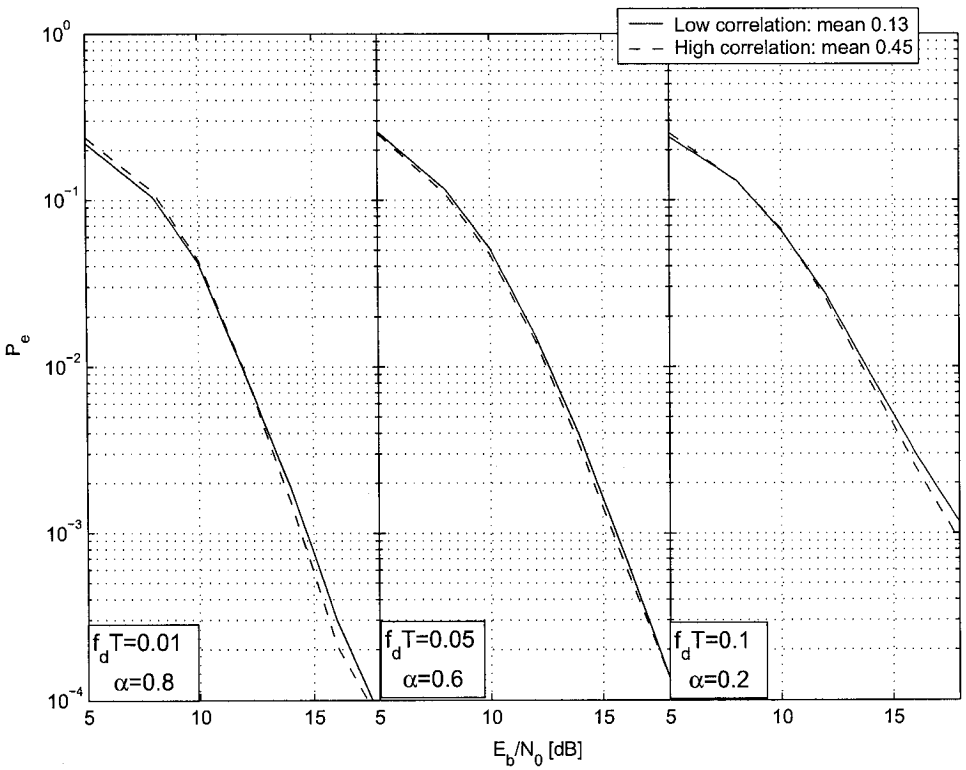

Figure 4.7: Performance of EigenIC dimension estimation scheme with correlated COST-207 channel

paths. For the graphs in Figures 4.7 and 4.8, the COST-207 channel was modified to include inter-path correlation (see Appendix B for details). The results show that the correlation did not degrade significantly the performance of the two algorithms, since the performance is very similar for correlation coefficients having a mean 0.13 versus a mean 0.45.

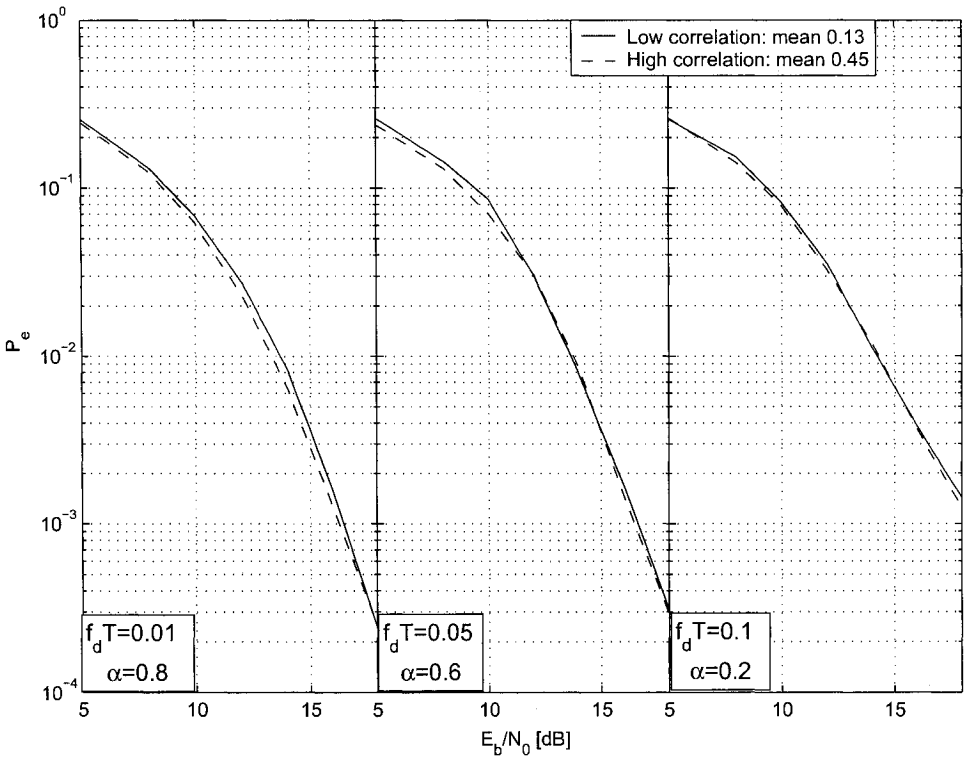

Figure 4.8: Performance of EigenEC dimension estimation scheme with correlated COST-207 channel

4.3 Results for Measured Channels

4.3.1 Typical Cellular Channels

In the following simulation results, the adaptive algorithms are subjected to real-life channel conditions. The channel measurements used in this section and the ones that follow include impairments such as multipath fading, intersymbol interference, correlation between channel paths, and additive correlated noise. More information regarding the channel data may be found in Appendix A and [Pat96]. This first set of results uses typical cellular channel measurements, a group of measurements which has the greatest number of significant eigenvalues. In general, the datasets from which the sample channels were picked have an effective orthogonal diversity of 2.8, and their average $D_{90\%}$ is 4. By contrast, D_c, the number of significant peaks in the power delay profile, is 5.7 on average.

The values chosen for α were those that produced the best results for that particular channel and algorithm. Note that the information criterion method did best with moderate α values, which likely corresponds to the fading rate of the channel. The energy criterion method produced the best results using the smallest window size possible. Figures 4.9(a) and (b) show that the two methods can be quite comparable when their parameters may be optimized.

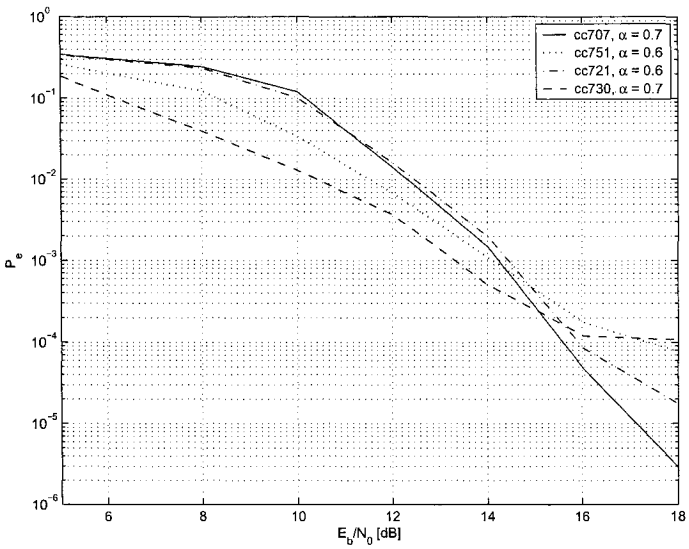

(a)

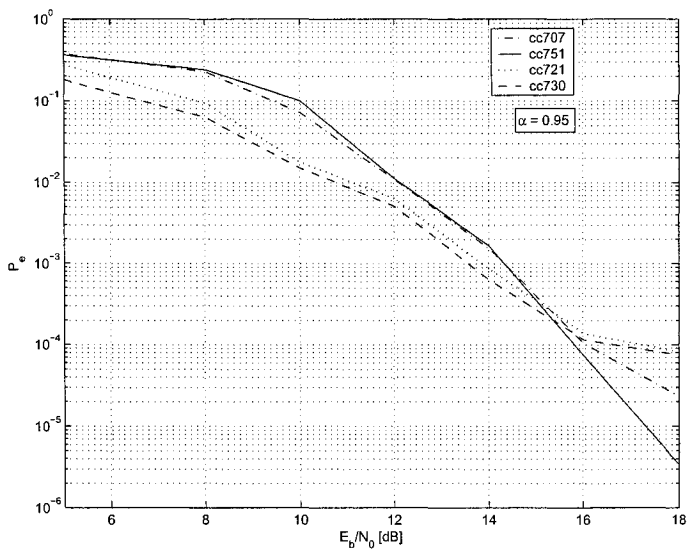

(b)

Figure 4.9: Performance of EigenIC and EigenEC algorithms, with conventional cellular channels

4.3.2 Microcellular Channels

A microcellular environment is one where there are more densely spaced transmitters, transmitting lower power and usually at a lesser height than conventional cellular base stations. To mimic this type of environment, channel measurements were taken in a busy downtown block, but where a line of sight existed to the receiver. In these channels there is usually one, powerful path in the power-delay profile, and the delay spread is short.

Results are shown in Figure 4.10 for two different instances of the microcellular channel measurements. The impairments in these channels were great, but the eigenanalysis detection algorithms seem to have the advantage over conventional differential detection. The three graphs for the uc2009 file are the ones with higher probability of error, and the lower three are for the uc2030 file. The reason for the slightly better performance is that the uc2009 had a more powerful line of sight path.

4.3.3 Indoor Channels

It is interesting now to examine the performance of the detection algorithms for indoor channels. For these channels as with the microcellular channels, the number of eigenvalues comprising 98% of the total signal energy, as well as the orthogonal effective diversity $D_{ortho-eff}$, is low (between 1 and 2 modes). Again, measured channel impulse reponse data is used as a time-varying filter process. There are measurements at 950

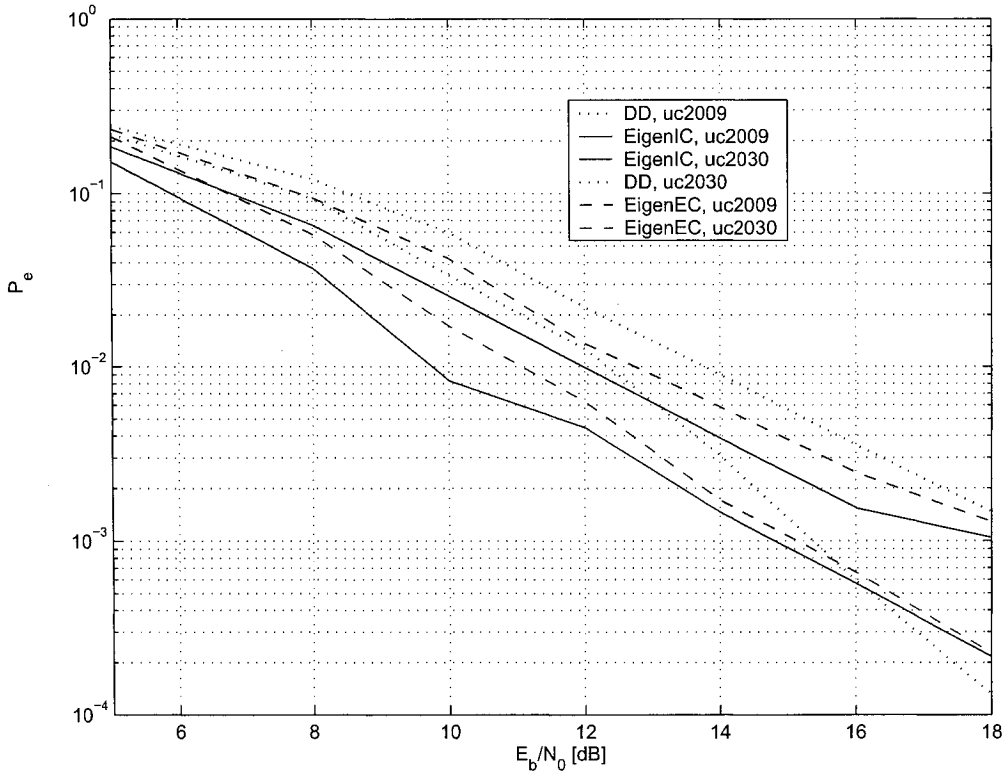

Figure 4.10: Performance of EigenIC and EigenEC algorithms, with microcellular channels

MHz and 40 GHz. In both cases, the channels were subject to multipath fading due to motion of objects and people in the indoor environment.

It is important to note that the points in time which exhibit the most effective orthogonal diversity are those where the power is shared most equally among the modes. In Figure 4.11, the channel displays the most orthogonal effective diversity at time 19, and in Figure 4.12, at time 34. The bottom halves of the graphs display the relative proportions of the two largest normalized eigenvalues, l'_1 and l'_2, for the indoor channel. Most of the time however, the first mode carries the greater proportion of the energy.

In the upper halves of the graphs, the probability of error is indicated for two detection schemes; conventional differential detection (dashed line) and eigenanalysis detection using the information criterion for dimension detection (solid line). The three sets of data represent the performance at 5 dB, 10 dB and 15 dB, from top to bottom. In both the 950 MHz and 40 GHz channels, the performance varies widely, due to the difference in channel conditions as time passes. The channel conditions for the 950 MHz are worse than for the 40 GHz channel. In Figure 4.12, the performance appears to be more strongly correlated with the total energy in all eigenvectors, than with the level of diversity. An exception to this rule is when the diversity increases significantly, in combination with a rise in total energy, for example at time 34 in Figure 4.12. Then the performance of conventional detection improves with respect to time 33, most likely due

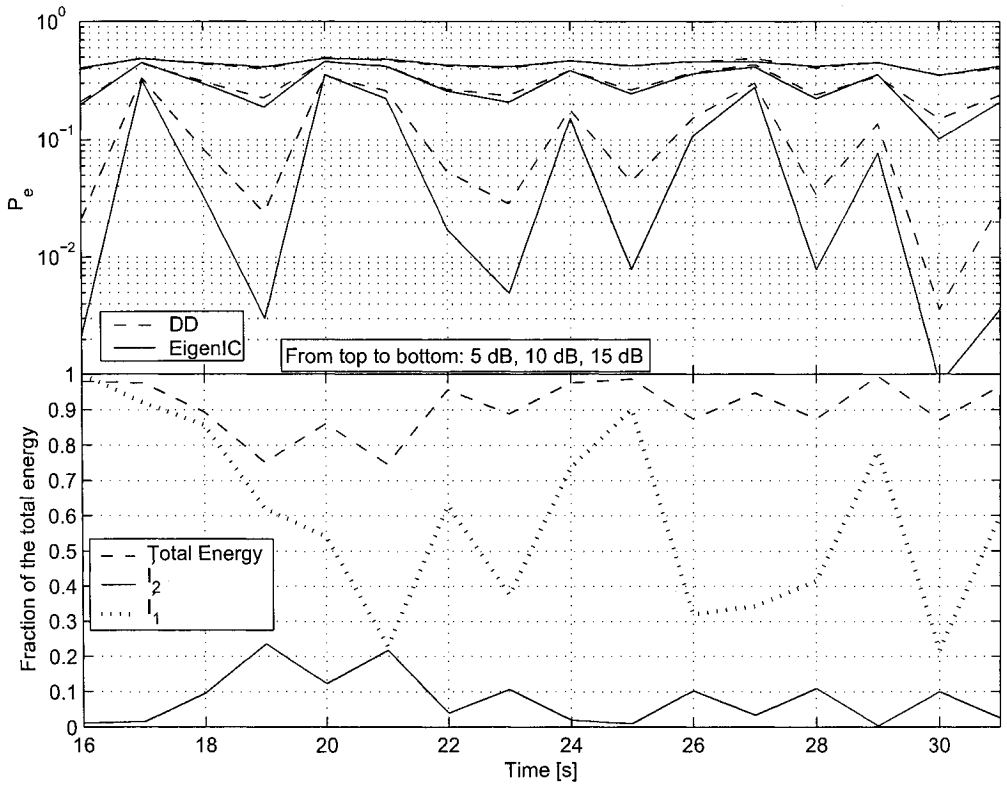

Figure 4.11: Performance of EigenIC with 950 MHz indoor channel data, indexed against normalized eigenvalues

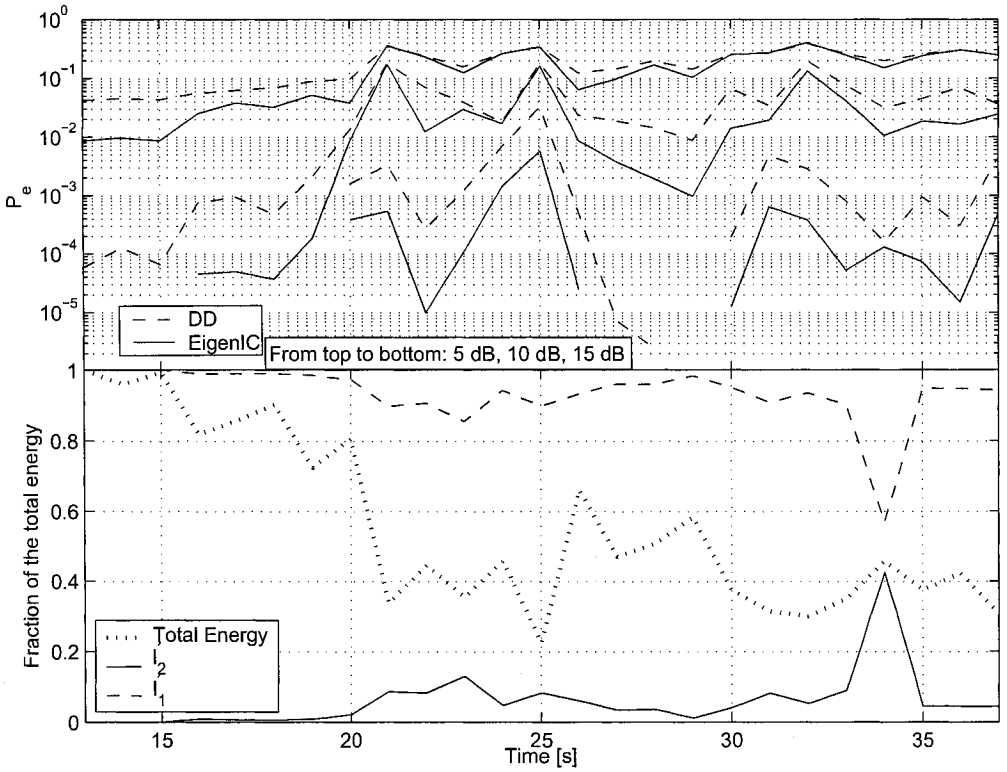

Figure 4.12: Performance of EigenIC with 40 GHz indoor channel data, indexed against normalized eigenvalues

to the increase in total energy. The eigenanalysis detector on the other hand, worsens, but only for high SNR (15 dB). It would seem that the eigenanalysis detector, while still outperforming conventional differential detection, is not benefitting from the increased diversity. When the SNR increased, a better estimate of the signal subspace dimension was probably found to be two or possibly three. But the second or third eigenvalues are less powerful, which might have meant their eigenvectors are more noise-occluded, causing the rise in P_e.

4.4 Algorithm Profiling Results

In the trade-off driven realm of electronics, cost is a necessary factor to consider regarding any part of a communications de-modulation algorithm. The above graphs show a performance improvement of the eigenanalysis algorithm over conventional differential detection techniques, but realistically, the eigenanalysis is much more computationally expensive. The conventional algorithm requires just K complex multiplications and $K-1$ real additions, as compared to $O(r^2K^2)$ or $O(r^3)$ for the energy criterion method and the information criterion method respectively, where r is the signal-noise subspace dimension and K is the size of the input vector $\mathbf{r}_n$. K is nominally between 10 and 30, depending on the delay spread and the sampling rate ($K = \lceil \tau_{max}/T_{delay} \rceil$, from Chapter 3).

In order to give a numerical example of the complexity, the eigendetection algorithms were implemented in the C programming language, compiled for a floating-point DSP, and profiled. Randomly-generated, channel-filtered symbol data was generated using MATLAB™, as it was in the simulations above, and output to a file. Part of this data file was loaded into the memory of the DSP, so that it could be directly accessed by the detection software, providing realistic input for the algorithm.

The hardware component of the test setup consisted of the Evaluation Module (EVM) 6701 from Texas Instruments (TI), comprising a TI TMS320C6701 floating point DSP.

The processor is run at 167 MHz, and is capable of up to 1600 MIPS. The simulation data was stored locally in the 1 Mb of on-chip memory. The algorithm was compiled using Code Composer Studio (CCS) with the highest level of compiler optimization ($-o3$), in full symbolic debug mode, and the assembly code was not modified.

The results given in Tables 4.2 and 4.3 indicate that the time spent by the algorithm on eigenstructure update is quite significant. These profiling results are based on just one dimension $D = 1$ as a baseline, since it was found from the simulations that the algorithm seems to choose $D = 1$ or 2 for the majority of the iterations. The eigendecomposition complexity increases as $O(D^3)$, so for $D = 2$, the number of CPU cycles could be estimated to be 8 times as many. Even still, the eigendecomposition would comprise at worst 25% of the total cycles involved. The reasons can easily be surmised: 1) the matrix multiplication operations involved in the eigenstructure update are on the order of K, which is larger than D, 2) the adaptive algorithm requires that orthogonal eigenvectors be generated, which is an expensive proposition using the Gram-Schmidt method, and 3) the computations are mostly complex outside of the eigenanalysis routine.

The total time to execute the algorithms was approximately 1.2 ms, this number being obtained by multiplication of the clock cycles by the clock speed, 167 MHz. If the particular communication standard implemented was CDMA IS-95, the maximum data rate would be 9.6 kbits/s, which is approximately 0.1 ms per bit. So in order to use

Table 4.2: Profiling Results for Information Criterion Method

Operation	Number of Cycles	Execution Time (ms)	% of algorithm
Eigenstructure Update	170633	1.0	85
Eigenanalysis	4090	0.02	2
Creation of Decision Variable	14395	0.09	13

Table 4.3: Profiling Results for Energy Criterion Method

Operation	Number of Cycles	Execution Time (ms)	% of algorithm
Eigenstructure Update	156208	0.94	89
Eigenanalysis	5691	0.03	3
Creation of Decision Variable	26012	0.16	13

this algorithm with the CDMA IS-95 standard and the TI TMS320C6701 chip, it would be necessary to either reduce the frequency of the eigenvector/eigenvalue updates, or increase the algorithm efficiency.

4.5 Conclusion

In this chapter, performance and profiling results were presented for the eigenanalysis detection algorithms previously outlined. The simplified algorithm with fixed D was shown with coherent detection, and the algorithm fared well given the lack of coding

and equalization. However, at higher fading rates, the performance degraded drastically, and even more so with QPSK. The higher dimensions detracted from the performance of these algorithms, despite the fact that optimal detection benefits from each new dimension added. Differential PSK proved to be the most promising modulation scheme, and results were presented for both of the fully adaptive algorithms with COST-207 and COST-259 channels. The relative performance of the information criterion method and the energy criterion method depends on the channel; at high fading rates the energy criterion method fared better, while the information criterion method did better overall. The addition of correlation to the channel didn't seem to change the performance of either algorithm.

For microcellular channels, both algorithms outperformed conventional differential detection. The information criterion method showed an improvement of as much as 2 dB for microcellular channels. This method was shown for indoor channels at carrier frequencies of 950 MHz and 40 GHz, and the eigenanalysis algorithm was superior at moderate and higher signal to noise ratios.

Chapter 5

Conclusion

5.1 Thesis Summary

This thesis builds upon and brings together work done to date in several different areas: the eigenstructure of multipath fading channels, channel estimation via statistical signal processing, and signal subspace rank detection, and applies it to data demodulation. A first algorithm, the so-called information criterion method, used a straight eigendecomposition by the QR algorithm, followed by a determination of the dominant eigenvectors by the AIC criterion. The second algorithm used an integrated eigendecomposition and rank-determination method, called the energy criterion method, whereby the dominant eigenpairs were calculated iteratively using the Lanczos method, until the sum of the eigenvalue energies reached a certain threshold. Both of these methods are

built upon the concept of eigenstructure updating of a recursively generated autocorrelation matrix. The autocorrelation matrix carries both the modulated data as well as the channel information. Once the autocorrelation matrix yields its dominant eigenvectors and eigenvalues, they are used in a weighted sum decision variable to re-construct the binary transmitted data.

The indication of the performance simulations is that the benefits of the eigenanalysis detector begin when the signal-noise subspace dimension is determined to be low. Interestingly, channels which are deemed to have a higher orthogonal effective diversity (such as the conventional cellular channels) do not seem to be better-suited to the eigenanalysis approach, most likely due to the difficulty in a) estimating $\hat{\mathbf{R}}$, and b) estimating the signal-noise subspace dimension. Of course, even when the signal-noise subspace can be determined accurately, the signal eigenvectors still contain correlated noise. A whitening filter would help to mitigate the correlation of the noise, but again at the cost of greater complexity. The less energetic eigenvectors remain somewhat of an untapped resource. It is known that in the ideal case, the more eigenvectors that can be combined, the better. In practice, it turns out that when using estimates of the eigenvectors in the decision variable, using a greater number of dimensions most often hinders performance. The most promising use for the detector presented seems to be for indoor and microcellular channels, where the use of just one or two dominant

eigenvectors is justified.

5.2 Thesis Contributions

The contributions of this thesis are:

Algorithm Definition. In order to benefit from the dominant modes of the wireless, fading channel, the algorithm must be sufficiently nimble to add and drop modes from one iteration to the next. Previously reported algorithms ([Pat96] and [Lat97]) either: 1) always output a fixed number of modes, using the information criterion to refine the dimension to the minimum number of significant modes before combining, or 2) allow the eigenstructure update to occur with a variable number of modes, but do not specify in enough detail how the change in dimension (especially an increase) would occur. In this thesis, two adaptive, variable-dimension algorithms were developed, including keeping track of an extra signal-noise eigenvector to allow for an instant dimension increase.

Performance Simulations. Though the energy criterion method and the information criterion method of signal-noise subspace rank-determination had been previously defined in the context of detection, in this thesis they were implemented and compared with each other and against conventional detection techniques. Several different types of fading channels were used to give an idea of the full range of

performance.

Real-time Program Execution. The detector was implemented using C code for the purpose of obtaining real-time execution results on a typical floating-point DSP. The results show that unless there is a great improvement in the efficiency of processors, more work is needed to reduce the complexity of the algorithm.

5.3 Suggestions for Future Research Work

As there do seem to be performance gains to the eigenanalysis approach, it is worthwhile to attempt to lessen the computational load incurred by the eigenanalysis detection algorithm. It would be useful to try to de-couple the data from the eigenvectors, so that the eigenvectors and eigenvalues would need to be calculated less frequently than once per symbol. There is also the task of determining the period over which an eigenvector/eigenvalue update estimate would be valid, and how to adaptively determine that period. It seems reasonable that this period would be equivalent to the channel coherence time.

It could also be investigated whether the eigenstructure update could be made more efficient, with a negligible performance loss. There is an update algorithm [DeG92] that attempts to fold all the signal eigenvectors into one, and all the noise eigenvectors into another, so that only two eigenvector/eigenvalue pairs need to be tracked at once.

Appendix A

Empirical Channel Impulse Response Data

The datasets used in this thesis were furnished by the Communications Research Centre (CRC) in Ottawa, where experiments were conducted by Dr. Robert Bultitude and others [BB89][BMS89]. The data was collected using wideband channel sounding techniques. There are three categories of data available: cellular channel, microcellular channel, and indoor channel. A description of all the data and a detailed analysis of the statistical properties of these channels is provided in [Pat96].

A.1 Swept time-delay crosscorrelator technique

The channel sounding technique involves transmitting a wideband signal and cross-correlating with its time-reversed corresponding received signal. The result is a characterization of the channel impulse response amplitude and phase as a function of time.

The particular technique used to generate the data used in this thesis is the swept time-delay crosscorrelator technique, which is described in detail in [PDT91]. Essentially, the spread-spectrum signal is correlated with the same m-sequence as was used to perform the spreading. There is a deliberate difference in the clock speed between the transmitter and receiver, such that the receiver clock is slightly slower than the transmitter clock (for example, f_tx = 10 MHz and f_rx = 9.998MHz). The slightly reduced clock speed governs the speed of the local Pseudo Random Bit Sequence (PRBS) generator, which is provided to the correlator. The output of the correlator will have a bandwidth equal to the difference in frequency ($f_{tx} - f_{rx}$ = 2 KHz). A consequence of the bandwidth compression is that it takes a longer time to gather the data for one delay profile; there is a time scaling factor of $f_{tx}/(f_{tx} - f_{rx}) = 5000$. Equivalently it can be said that there are $f_{tx}/(f_{tx} - f_{rx})$ individual responses contained in one delay profile. A vehicle in motion receiving data using this technique needs to move slowly so that the channel would be fairly constant over the time necessary to collect one delay profile.

A.2 Description of Data

A.2.1 Typical Cellular Channels

For the gathering of the cellular channel data, a transmitter placed on the edge of the roof of a building, 78 m from the ground was used to transmit BPSK data. Each symbol was multiplied by a 127-element pseudo-random sequence with a rate of 10 Mcps, and modulated with a carrier frequency of 910 MHz. For the majority of the data, there is no line of sight path to the receiver. The receiver was located in a street with moderate traffic (O'Conner, Lyon and Metcalfe in Ottawa). The receiver is mounted on a track on the roof of a stationary vehicle, and was moved along the track at a rate of approximately 0.28 m/s over a distance of 4.575 m. At each interval of 3.57 cm (127.7 ms), one complete channel impulse response was measured. The equipment is able to resolve the incoming signals with a resolution of 100 ns. Given the velocity of the receiver and the carrier frequency, the maximum doppler shift is 0.85 Hz. The maximum observed delay is about $3\mu s$.

A.2.2 Microcellular Channels

A microcellular communications system is one where the transmitters are fixed at locations lower to the ground than in a conventional cellular system, and are lower-powered and more densely spaced. As in the previous measurements, the receiving antenna was

on the roof of a stationary vehicle (3.5 m from the ground), and moved along a track at a velocity of 0.28 m/s over a distance of 4.575 m. The transmitting antenna was placed on the roof of another stationary vehicle, in a street on a city block of downtown Ottawa. In all cases, a line-of sight path existed. Less time dispersion was observed in these experiments than in the cellular channel experiments.

A.2.3 Indoor Channels

The indoor measurements were taken at two different carrier frequencies; 950 MHz and 40 GHz. The 950 MHz measurements were taken at CRC inside building 2D, which is a typical office setting with office furniture and cubicle walls of height 1.8 m. Each symbol was multiplied by a 63-element pseudo-random sequence with a rate of 40 Mcps, for a resolution of 25 ns. There was no line of sight path.

For the 40 GHz measurements, the same pseudo-random sequence and transmission rate was used as for the measurments at 950 MHz. The location was the third floor of building 2A at CRC, where the transmitter was placed in the center of a room, and the receiver was placed near the door of a second room, adjacent the first.

Appendix B

Simulation of Mobile Radio Channels

B.1 Channel Simulators

Two types of software channel simulator were used to analyze the detector performance: a conventional channel model which considers each individual multipath ray, and a simulator that uses actual measured channel impulse response data.

B.1.1 Conventional Multipath Simulator

The conventional way of simulating a Rayleigh fading channel is well described in [Rap96]. The method begins with the generation of an in-phase and a quadrature

Gaussian noise vector. The power of each multpath component is determined by the variance of the complex generated Gaussian noise. These vector may be taken as time sequences or frequency spectra; in the latter case, they must be multiplied by the fading spectrum, in the former case, filtered with the fading process. The result of the multiplication or filtration should be converted to the time domain if it is not there already, and the magnitude of the time series taken. This time series (call it $g_i(t)$) is the time representation of a single fading process; one is required for each path i in the channel. The flat fading gain a_i may be applied as a multiplicative factor to each series $g_i(t)$. To use the $g_i(t)$, the incoming signal must be duplicated once for each path. Then the duplicates are delayed by their respective time delays, multiplied sample for sample by the series $g_i(t)$, and added together to form the resultant signal.

The COST models were developed to simulate Group Special Mobile (GSM) products. It specifies typical fading processes in terms of its path powers and delays, for different environments. The COST-207 and COST-259 models for a typical urban channel are shown in Table B.1. COST-207 has 12 paths and a short delay spread while COST-259 has 20 paths and a relatively long delay spread.

The fading spectrum used in the simulations is a classical Clarke and Gans fading spectrum [Rap96]; see figure B.1.

Table B.1: GSM Typical Urban Channel Models

COST-207 Model		COST-259 Model	
Delay (μs)	Power	Delay (μs)	Power
0	0.0904	0	0.2692
0.027	0.1134	0.217	0.1738
0.054	0.2271	0.512	0.0977
0.082	0.1433	0.514	0.0955
0.109	0.1138	0.517	0.0955
0.163	0.0718	0.674	0.0708
0.190	0.0454	0.882	0.0457
0.244	0.0718	1.230	0.0234
0.325	0.0571	1.287	0.0204
0.407	0.0286	1.311	0.0195
0.434	0.0180	1.349	0.0182
0.678	0.0227	1.533	0.0126
-	-	1.535	0.0126
-	-	1.622	0.0105
-	-	1.818	0.0071
-	-	1.836	0.0069
-	-	1.884	0.0062
-	-	1.943	0.0055
-	-	2.048	0.0045
-	-	2.140	0.0037

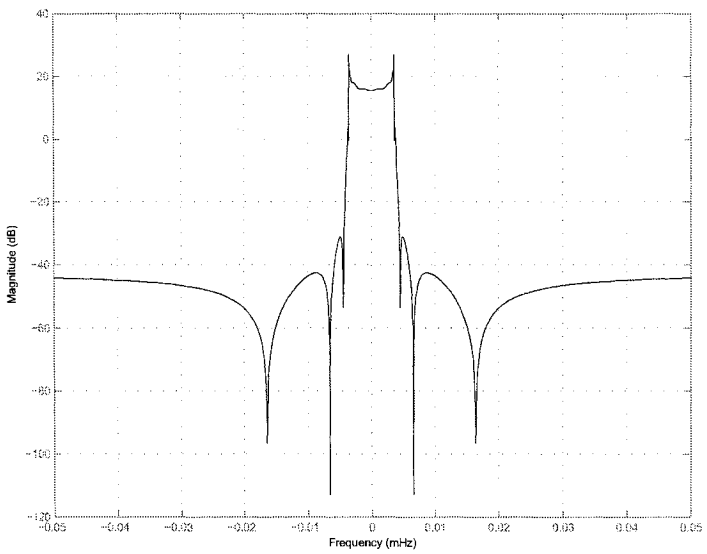

Figure B.1: Doppler Filter Magnitude Response

B.1.2 Orthogonal Multipath Simulator

The conventional multipath simulator is an implementation of the equation:

$$\mathbf{h}_n = \mathbf{P}\mathbf{a}_n + \boldsymbol{v}_n \tag{B.1}$$

As discussed in Chapter 2, the matrix $\mathbf{P}$ consists of non-orthogonal vectors which, when weighted by the complex path gains $\mathbf{a}_n$, represent the impulse response of each path in the channel. The autocorrelation of this matrix is:

$$\mathbf{R}_s = \mathbf{P}\mathbf{a}_n\mathbf{a}_n^H\mathbf{P}^T = \mathbf{V}\mathbf{g}_n\mathbf{g}_n^H\mathbf{V}^H \tag{B.2}$$

where $\mathbf{V}$ are the orthogonal vectors analogous to $\mathbf{P}$, and $\mathbf{g}_n$ are the orthogonal complex gains analogous to $\mathbf{a}_n$.

If there is correlation between the path gains, the matrix $\mathbf{R}_a = \mathbf{a}_n\mathbf{a}_n^H$ is no longer a diagonal matrix. In order to simulate a channel with correlated path gains, a correlated $\mathbf{R}_a$ can be created. Then, by finding the autocorrelation matrix $\mathbf{R}_s$ and its eigendecomposition, the orthogonal eigenvectors and eigenvalues may be found. These may be used as shown in Figure B.2 to simulate a correlated channel. The eigenvalues were used as the average power of each randomly generated orthogonal complex gain. The same Doppler spectrum as above was used to filter the random signal.

The matrix $\mathbf{R}_a$ was created using $\mathbf{a}_n\mathbf{a}_n^H$ as the main diagonal, and filling out the rest of the matrix hermetian symmetrically with random phase, typical magnitude correlation

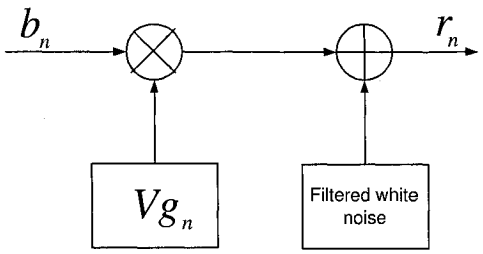

Figure B.2: Block Diagram of Alternate Simulation Method

values.

B.1.3 Measured Impulse Response Data Simulator

As previously mentioned, the channel impulse response can be thought of as a set of time-varying linear filters. For the experiments of Chapter 4, a number of impulse responses were available which were in effect samples of the channel random process. In Appendix 2, the measured impulse response data and its method of collection are discussed in more detail.

To put these real-world channel impulse response measurements to use in a simulated environment, a time-varying filter was created. The filter coefficients were derived from the sample values of the measured impulse response data. Since the data was created by sampling at a rate of 8 samples/chip, a decimation in delay by a factor of 4 was performed to give 2 samples/chip, the simulation sampling rate. The first few samples, which lead

up to the response, were removed, and the data was truncated after the response mostly dies out. The data was then interpolated in time by a factor of 101. The rationale for the interpolation is as follows. While the data was being collected, one channel impulse response (CIR) was measured every 0.1277 s, and one symbol period is 12.7 ms. That makes roughly 10100 symbols sent per CIR characterization. By interpolating the data by 101, there is a CIR every 100 symbols. One CIR can be used to filter every symbol in the simulation, effectively raising the fading rate by approximately 100 times. During data collection the receiver was in motion at a rate of 1 km/h, so with the increase of a factor of 100, the normalized fading rate is approximately 0.001.

The normalized data values became the set of coefficients, one of which was used per symbol. When the end of the set of coefficients was reached, the cycle began again at the start.

Bibliography

[Baj68] A.S. Bajwa. UHF wideband statistical model and simulation of mobile radio multipath propagation effects. *IEE Proceedings*, 47:957–1000, July–August 1968.

[Bal82] J.R. Ball. A real-time fading simulator for mobile radio. *The Radio and Electronic Engineer*, 52(10):475–478, October 1982.

[BB89] R.J.C. Bultitude and G.K. Bedal. Propagation characteristics on microcellular urban mobile radio channels at 910 MHz. *IEEE Journal on Selected Areas in Communications*, 7(1):31–39, January 1989.

[BD91] W.R. Braun and U. Dersch. A physical mobile radio channel model. *IEEE Transactions on Vehicular Technology*, 40(2):472–482, May 1991.

[Bel63] P. A. Bello. Characterization of randomly time-variant linear channels. *IEEE Transactions on Communications Systems*, 11:360–393, December 1963.

[BMS89] R.J.C. Bultitude, S.A. Mahmoud, and W.A. Sullivan. A comparison of indoor radio propagation characteristics at 910 mhz and 1.75 ghz. *IEEE Journal on Selected Areas in Communications*, 7(1):20–30, January 1989.

[BNS78] J.R. Bunch, C.P. Nielsen, and D.C. Sorensen. Rank-one modification of the symmetric eigenproblem. *Numerische Mathematik*, 31:31–48, 1978.

[BSK85] A. M. Bruckstein, T.-J. Shan, and T. Kailath. The resolution of overlapping echoes. *IEEE Transactions on Acoustics, Speech, and Signal Processing*, 33(6):1357–1367, December 1985.

[Cla68] R.H. Clarke. A statistical theory of mobile-radio reception. *The Bell System Technical Journal*, 47:957–1000, July–August 1968.

[Cox72] D.C. Cox. Delay doppler characteristics of multipath propagation at 910 MHz in a suburban mobile radio environment. *IEEE Transactions on Antennas and Propagation*, 20(5):625–635, 1972.

[DeG92] R.D. DeGroat. Noniterative subspace tracking. *IEEE Transactions on Signal Processing*, 40(3):571–577, March 1992.

[DR90] R.D. DeGroat and R.A. Roberts. Efficient, numerically stabilized rank-one eigenstructure updating. *IEEE Transactions on Acoustics, Speech, and Signal Processing*, 38(2):301–316, February 1990.

[Fec93] S. A. Fechtel. A novel approach to modeling and efficient simulation of frequency-selective fading radio channels. *IEEE Journal on Selected Areas in Communications*, 11(3), April 1993.

[GL89] G.H. Golub and C.F. Van Loan. *Matrix Computations.* Johns Hopkins Press, Baltimore, MD., second edition, 1989.

[Has93a] H. Hashemi. Impulse response modelling of indoor radio propagation channels. *IEEE Journal on Selected Areas in Communications*, 11(7):967–978, September 1993.

[Has93b] H. Hashemi. The indoor radio propagation model. *Proceedings of the IEEE*, 81:943–968, July 1993.

[JFT+72] T.L. Johnston, S.B. Fine, G. L. Turin, F.D. Clapp, and D. Lavry. A statistical model of urban multipath propagation. *IEEE Transactions on Vehicular Technology*, 21(1):1–9, February 1972.

[KM99] V.-P. Kaasila and A. Mammela. Bit error probability of a matched filter in a Rayleigh fading multipath channel in the presence of interpath and intersymbol interference. *IEEE Transactions on Communications*, 47:809–812, June 1999.

[KY96] A. Kavcic and B. Yang. Adaptive rank estimation for spherical subspace trackers. *IEEE Transactions on Signal Processing*, 44(6):1573–1579, June 1996.

[Lat97] J.-M. Latapy. Modes orthogonaux d'une réponse impulsionelle sur canal radio mobile. Master's thesis, Ecole Nationale Supérieure de Télecommunications, 1997.

[LT94] P. Lascaux and R. Théodor. *Analyse numérique matricielle appliquée à l'art de l'ingénieur, tomes 1 et 2.* Masson, 1993-1994.

[Och87] H. Ochsner. Direct-sequence spread-spectrum receiver for communication on frequency-selective fading channels. *IEEE Journal on Selected Areas in Communications*, 5(2):188–193, February 1987.

[Par80] B.N. Parlett. *The symmetric eigenvalue problem.* Prentice-Hall, New Jersey, 1980.

[Pat96] F. Patenaude. *Modélisation et détection par analyse propre pour les canaux multivoies avec évanouissements.* PhD thesis, University of Ottawa, 1996.

[PDT91] J.D. Parsons, D.A. Demery, and A.M.D. Turkmani. Sounding techniques for wideband mobile radio channels: A review. *IEE Proceedings*, 138:327–333, October 1991.

[PLC99] F. Patenaude, J. Lodge, and J.-Y. Chouinard. Eigen analysis of wide-band fading channel impulse responses. *IEEE Transactions on Vehicular Technology*, 48:593–606, March 1999.

[Pro01] J. G. Proakis. *Digital Communications.* McGraw-Hill, New York, fourth edition, 2001.

[Rap96] T. S. Rappaport. *Wireless Communications.* Prentice Hall, New Jersey, 1996.

[Ste87] S. Stein. Fading channel issues in system engineering. *IEEE Journal on Selected Areas in Communications*, 5(2), February 1987.

[Ste88] A. O. Steinhardt. Householder transforms in signal processing. *IEEE Signal Processing Magazine*, 5(3):4–12, July 1988.

[SW94] H. Stark and J.W. Woods. *Probability, Random Processes and Estimation Theory for Engineers.* Prentice Hall, New Jersey, second edition, 1994.

[SZ00] M. Stojanovic and Z. Zvonar. Differentially coherent diversity combining techniques for DPSK over fast Rayleigh fading channels. *IEEE Transactions on Vehicular Technology*, 49(5):1928–1933, September 2000.

[T. 00] T. K. Moon and W. C. Stirling. *Mathematical Methods and algorithms for signal processing.* Prentice-Hall, NJ, 2000.

[TDP91] A.M.D. Turkmani, D.A. Demery, and J.D. Parsons. Measurements and modeling of wideband mobile radio channels at 900 MHz. *IEE Proceedings*, 138:447–457, October 1991.

[Tur80] G. L. Turin. Introduction to spread-spectrum antimultipath techniques and their application to urban digital radio. *Proceedings of the IEEE*, 68(3), March 1980.

[W. 02] W. H. Press and S. A. Teukolsky and W. T. Vetterling and B. P. Flannery. *Numerical Recipes in C, The Art of Scientific Computing.* Cambridge University Press, New York, second edition, 2002.

[WK85] M. Wax and T. Kailath. Detection of signals by information theoretic criteria. *IEEE Transactions on Acoustics, Speech, and Signal Processing*, 33(2), April 1985.

[YG94] B. Yang and F. Gersemsky. An adaptive algorithm of linear computational complexity for both rank and subspace tracking. *Proc. IEEE ICASSP'94*, pages IV33–IV36, April 1994.